Physics of the Earth and Planetary Interiors 171 (2008) 92–111

Contents lists available at ScienceDirect

Physics of the Earth and Planetary Interiors

journal homepage: www.elsevier.com/locate/pepi

Comparison of Eulerian and Lagrangian numerical techniques for the Stokes equations in the presence of strongly varying viscosity

Y. Deubelbeiss[a,b,*], B.J.P. Kaus[b,c]

[a] Institute for Mineralogy and Petrology, Department of Earth Sciences, ETH Zurich, NW E75.1, Clausiusstrasse 25, 8092 Zurich, Switzerland
[b] Geophysical Fluid Dynamics, Department of Earth Sciences, ETH Zurich, 8093 Zurich, Switzerland
[c] Department of Earth Sciences, University of Southern California, Los Angeles, CA 90089-0740, USA

ARTICLE INFO

Article history:
Received 24 October 2007
Received in revised form 22 April 2008
Accepted 30 June 2008

Keywords:
Finite difference methods
Staggered grid
Stream function
Rotated staggered grid
Finite element methods
Stokes equations
Geodynamic modeling
Analytics
Numerical methods
Lagrangian and Eulerian grids

ABSTRACT

Numerical modeling of geodynamic problems typically requires the solution of the Stokes equations for creeping, highly viscous flows. Since material properties such as effective viscosity of rocks can vary many orders of magnitudes over small spatial scales, the Stokes solver needs to be robust even in the case of highly variable viscosity. A number of different techniques (e.g. finite difference (FD), finite element (FE) and spectral methods) are presently in use. The purpose of this study is to evaluate the accuracies of several of these techniques. Specifically, these are staggered grid, stream function and rotated staggered grid finite difference method (FDM) and an unstructured finite element method (FEM) with various arrangements of elements. Results are compared with two different analytical solutions: (1) stress distribution inside and around strong or weak viscous inclusions subjected to pure-shear and (2) density-driven flow of a simple two-layer system. The comparison shows, in case of the three FD techniques, that the manner in which viscosity parameters are defined in the numerical grid plays an important role. The application of different viscosity interpolation methods yields differences in accuracy of up to one order of magnitude. In case of the FEM, results show that the arrangement of the elements in the region of material interfaces and the way in which material properties are defined also strongly affects the accuracy.

We derived a 1D analytical solution for a simple physical model where an interface separates two domains of different viscosities. If the interface is located between two nodal points the effective viscosity for this cell is a harmonic average of the two viscosities weighted according to the fraction of each material in this cell. Numerically, fractions were evaluated by using markers bearing the material property information.

The 2D problem differs from the 1D problem in that in 2D, two viscosities are necessary for a conservative FD formulation, one in the center and one at nodal points of a cell. Harmonic (in some cases geometric) averaging of the viscosity from markers to center points and a second harmonic averaging from center to nodal points is shown to give the most accurate FD results. In presence of density variations additionally a marker based arithmetic average for density should be applied. Results obtained by an unstructured FEM with elements following exactly the material boundaries show accuracies of one to two orders of magnitude better then results produced by Eulerian FD or FE methods. If viscosities are directly sampled at integration points, however, the FEM is less accurate than FD methods. Elementwise averaging of viscosities yields similar accuracies for both methods.

1. Introduction

Numerical modeling of geodynamic processes on geological timescales requires solving of Stokes-like equations regardless of whether the rheology is viscous, non-Newtonian, visco-elastic or visco-elasto-plastic (e.g. Gerya and Yuen, 2003, 2007; Braun and Sambridge, 1994; Schmeling and Jacoby, 1981; Moresi et al., 2002, 2003, 2007; Zhong et al., 2007; Schmalholz et al., 2001; Vasilyev et al., 2001; Fullsack, 1995; Kaus et al., 2004). A major complication in numerically solving such problems is that the effective material properties of rocks vary many orders of magnitudes due to either changes in temperatures or differences in composition. For example, the effective viscosity of olivine has an Arrhenius-type temperature dependence of the form $\eta \propto \exp(Q/(nRT))$. Representative values are $Q \approx 400\,\mathrm{kJ/mol}$, $R = 8.3145\,\mathrm{J/(K\,mol)}$. This results in an effective viscosity contrast between near surface conditions

* Corresponding author at: Institute for Mineralogy and Petrology, Department of Earth Sciences, ETH Zurich, NW E75.1, Clausiusstrasse 25, 8092 Zurich, Switzerland. Tel.: +41 44 633 76 53; fax: +41 44 633 10 65.
E-mail address: yolanda.deubelbeiss@erdw.ethz.ch (Y. Deubelbeiss).

0031-9201/$ – see front matter © 2008 Elsevier B.V. All rights reserved.
doi:10.1016/j.pepi.2008.06.023

($T \approx 400$ K) and the upper mantle ($T \approx 1600$ K) of $\eta/\eta_0 \sim 10^{39}$ Pa s. Similarly, to solve the problem of propagation of basaltic dikes ($\eta \approx 100$ Pa s; Shaw, 1969) through the visco-elastic upper crust ($\eta \approx 10^{23}$ Pa s; Ranalli, 1995), the numerical method should be capable of handling viscosity contrasts of 10^{21} over length scales of tens of meters. Similar difficulties, although slightly less dramatic, occur in visco-plastic problems, in which the effective viscosity inside a shear zone typically is several orders of magnitude smaller than outside the shear zone (with a width of a few numerical grid points).

The Stokes problem, in the case of constant viscosity, is one of the classical problems in numerical mathematics, as it is the prototype equation for saddle-point problems. Therefore, numerous methods have been developed to solve the equations efficiently (see e.g. Elman et al., 2005, for an overview). Unfortunately these methods are insufficiently studied for cases where viscosity is strongly varying as the Stokes equations become very ill-conditioned. This makes it difficult to directly apply those methods and so far almost no theoretical work seems to have been performed for geodynamically relevant cases.

Moresi and Solomatov (1995) developed a multigrid method for 2D convection problems capable of handling viscosity variations of up to 14 orders of magnitude. Although this is an impressive result, the reason why a solution could be found with iterative methods could be related to the relatively smooth variations in viscosity (which was also found by Auth and Harder, 1999; Kameyama et al., 2005; Choblet, 2005). Sharp gradients in effective viscosities cause a deterioration in the performance of numerical methods, and may also lead to non-convergence of solutions (e.g. Tackley, 2000; Choblet, 2005; Albers, 2000; Trompert and Hansen, 1996). Indeed, it was shown by Moresi et al. (1996), in which direct and multigrid methods were compared with analytical solutions, that the accuracy of the solution depends on the local (elementwise) variation of viscosity. If the jump in material properties occurs exactly at the element boundary, the errors in velocity and pressure are relatively independent of the total viscosity contrast. If the jump in material properties occurs inside an element, however, errors increased by more than two orders of magnitude. Finally, they demonstrated that the errors in velocity are one to two orders of magnitudes smaller than the errors in pressure.

This was also found in Schmid (2002), in which the dynamic pressure solution around circular and elliptic inclusions was compared with a numerical FE solution. Schmid found that it was necessary to use an unstructured FEM, together with higher order (Q_2P_{-1}) shape functions (instead of the linear shape functions employed by, e.g. Moresi et al., 1996) to obtain accurate pressure solutions.

If one is interested in accurate velocity solutions only, most methods seem to be reliable provided no strong viscosity contrasts occur within an element. If one, however, is also interested in accurate dynamic pressures one has to consider possible effects of the definition of material properties in numerical grids.

Motivation for the development of numerical techniques that accurately resolve the pressure field during deformation comes from a variety of sources:

- It has become more common to track the pressure–temperature evolution of rocks in numerical codes of lithospheric deformation, for the purpose of comparison with observed data (e.g. Toussaint et al., 2004; Jamieson et al., 2006; Burg and Gerya, 2006). Since tectonic stress can be significant under certain circumstances (Petrini and Podladchikov, 2000), it is crucial to use dynamic pressure instead of lithostatic load for reconstructing P–T paths.
- Treatment of plasticity requires knowledge of the absolute values of stress. Using dynamic pressure for this improves the sharpness of shear bands (Gerya and Yuen, 2007). Moreover, one of the interesting features of Mohr–Coulomb plasticity is that it lowers the pressure inside the shear-band, which makes this rheology different than that of ductile shear zones (Vermeer, 1990; Mancktelow, 2006).
- Fluid flows down pressure gradients. Lowering the solid pressure locally thus focuses fluids into brittle shear zones, a mechanism that is often invoked to explain strain weakening (Huismans and Beaumont, 2002). Self-consistent modeling of such strain-weakening processes requires coupling of solid deformation with Darcy-type flow, and hence requires accurate dynamic pressure solutions (Morency et al., 2007).
- Melt migration through compacting, two-phase flow materials requires solving equations for the fluid and the solid matrix (e.g. McKenzie, 1984; Scott and Stevenson, 1986). With few notable exceptions (Katz et al., 2006; Scott, 1988; Spiegelman, 2003) most formulations restrict their analysis to cases in which the solid matrix is rigid. Whereas this greatly simplifies the analysis, a full description of the problem seems necessary for certain problems such as shear-localization in partially molten rocks (Katz et al., 2006), and requires accurate stresses in the solid matrix.

These applications demonstrate that it is important to understand the accuracy of numerical methods for Stokes flow in the presence of large variations in material properties. As it is described above, the studies of Moresi et al. (1996) and Schmid (2002) show that the FEM would be an appropriate tool to solve such problems. Its disadvantage is that it requires exact knowledge of locations of material interfaces; there are many situations in geodynamic modeling in which this is not the case, or in which it would be prohibitively expensive to dynamically generate such a mesh. Examples are cases in which melt spontaneously localizes into small zones (e.g. Connolly and Podladchikov, 2007), models with shear-localization (e.g. Kaus and Podladchikov, 2006; Buiter et al., 2006) and geodynamic models of multi-phase lithospheric-scale deformation (e.g. Gorczyk et al., 2007; Fullsack, 1995). The most practical methods for such problems, in particular in 3D, seem to be Eulerian or arbitrary Lagrangian–Eulerian methods with quasi-structured grids as they are routinely employed in the mantle convection community.

Among the described methods there are other methods, which might be potentially powerful in tracking free surfaces such as an interface between two different materials. Some examples are Level-set, boundary integral or volume-of-fluid methods (Mühlhaus et al., 2007; Sussman et al., 1994). Each of this methods has its own advantages and disadvantages. The volume-of-fluid method has difficulties to handle merging and folding interfaces. It would require reordering of the interface points and would result in complex programming. Boundary integral methods require the integral description of the equations and might become difficult to implement if viscosity is temperature dependent or if phase transitions occur. While all these interface tracking methods work very well for simple problems with only few different materials and interfaces, its implementation for multi-phase problems is insufficiently studied.

Thus the objective of this study is to obtain a better insight in the accuracies of the dynamic pressure and velocity solution for various 2D FDM and FEM of the Stokes equations. It has been demonstrated that FD and finite volume methods are very efficient in solving multi-component geodynamic problems (e.g. Gerya and Yuen, 2007; Schott et al., 2000; Weinberg and Schmeling, 1992; Katz et al., 2006). The main aims of the present work are

- To demonstrate that, with relatively simple suggestions, the accuracy of the pressure solution of the Stokes solver can be improved. Many authors use FDM to model geodynamical problems. Mod-

els using FDM require the application of interpolation schemes; if the interpolation is carefully chosen the accuracy of solution can be improved by almost one order of magnitude.
- To compare the accuracy of FEM with those of FDM. Of interest is also how accurate FEM soltions are if phase boundaries are not exactly followed by the mesh (i.e. Eulerian FEM).

We employ three different FD formulations: (1) a staggered grid velocity–pressure FDM, (2) a stream function FDM, and (3) a rotated staggered grid velocity–pressure FDM, which was recently demonstrated to be effective for simulating wave propagation in heterogeneous rocks and an unstructured FEM using different element setups. Numerical solutions are compared with analytical solutions for the flow around circular inclusions of different viscosity and with analytical solutions of density-driven flow. The staggered grid and stream function FDM require viscosities to be defined both at centers and at nodal points of a cell, while the rotated staggered grid FDM only requires viscosity defined at center points. We demonstrate that the manner in which viscosities are defined at these locations is of extreme importance for the accuracy of the overall solution. In case of the FEM the accuracy is affected by the type of mesh as well as by the averaging method of viscosity.

In the following, we begin by describing the governing equations. We than illustrate the problem of viscosity interpolation with a 1D problem for which an analytical solution can be found. We continue with the description of the numerical methods, definition of benchmark studies and a discussion of our results and conclusions.

2. Governing equations

The governing continuum mechanics equations for slowly moving Newtonian viscous, incompressible flow are the Stokes equations (e.g. Turcotte and Schubert, 1982; Schubert et al., 2001):

$$\frac{\partial v_i}{\partial x_i} = 0, \tag{1}$$

$$\frac{\partial \sigma_{ij}}{\partial x_j} = \rho g_i, \tag{2}$$

$$\tilde{\sigma}_{ij} = 2\mu \dot{\varepsilon}_{ij}, \tag{3}$$

$$\dot{\varepsilon}_{ij} = \frac{1}{2}\left(\frac{\partial v_i}{\partial x_j} + \frac{\partial v_j}{\partial x_i}\right), \tag{4}$$

$$\sigma_{ij} = -\delta_{ij} P + \tilde{\sigma}_{ij}, \tag{5}$$

where v_i denotes velocity, $\tilde{\sigma}_{ij}$ deviatoric stress, σ_{ij} total stress, P pressure, μ Newtonian viscosity, ρ density, g_i gravitational acceleration, δ_{ij} the Kronecker delta, and the Einstein summation convention is assumed.

3. 1D analytical solution and its numerical application

To obtain insight in the accuracy of numerical solutions in the presence of strong viscosity variations, we derive an analytical solution for a quasi 1D case, which we employ to estimate the accuracy of numerical solutions. We consider a thin bar of length L that is composed of two regions with different constant viscosity separated by an interface. The system is subjected to stress boundary conditions (Fig. 1).

3.1. Analytical solution

3.1.1. General derivation

For the given setup, we can assume that shear stresses are zero. In this case, the governing equations (Eqs. (1)–(5)) simplify to

$$\frac{\partial v_x}{\partial x} + \frac{\partial v_z}{\partial z} = 0, \tag{6}$$

$$\frac{\partial \sigma_{xx}}{\partial x} = 0, \tag{7}$$

$$\frac{\partial \sigma_{zz}}{\partial z} = 0, \tag{8}$$

$$\sigma_{xx} = -P + 2\mu \frac{\partial v_x}{\partial x}, \tag{9}$$

$$\sigma_{zz} = -P + 2\mu \frac{\partial v_z}{\partial z}, \tag{10}$$

where Eq. (6) represents conservation of mass, Eqs. (7) and (8) conservation of momentum, and Eqs. (9) and (10) define the rheology. The boundary conditions are constant stress on the right hand side, free slip at the left hand side and stress free on top and at the bottom (i.e. $\sigma_{zz} = 0$). Integrating Eq. (8) versus z, combined with the stress free upper boundary condition yields $\sigma_{zz} = 0$. From this and Eq. (10) we obtain $P = 2\mu(\partial v_z/\partial z)$ or, after using Eq. (6), $P = -2\mu(\partial v_x/\partial x)$. Thus the resulting force balance in x-direction is

$$\frac{\partial \sigma_{xx}}{\partial x} = 0, \tag{11}$$

$$\sigma_{xx} = 4\mu \frac{\partial v_x}{\partial x}. \tag{12}$$

3.1.1.1. Velocity distribution. Integrating Eq. (11) versus x yields $\sigma_{xx} = 4\mu(\partial v_x/\partial x) = \text{constant}$. From this follows that v_x should be linear versus x. If the velocity at the interface, located at a, is $v_x^a = v_x(x = a)$, the velocities at the left and right boundary are

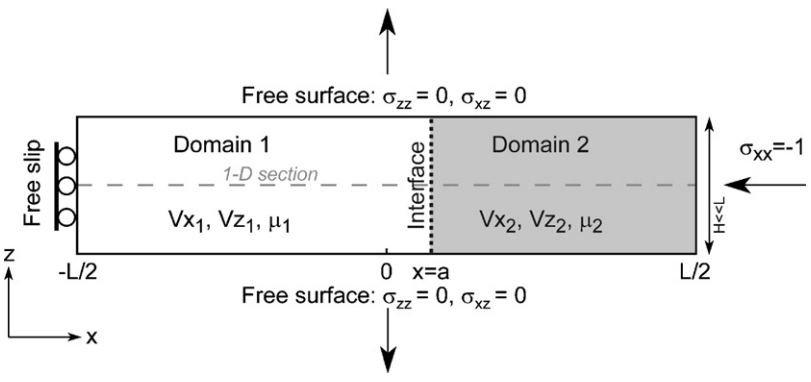

Fig. 1. Thin bar undergoing pure shear deformation. The bar is composed of two domains (1 and 2) with different viscosities μ_1 and μ_2, separated by a sharp interface. Constant stress boundary conditions are applied at the right hand side, a free surface is considered at the top and bottom boundaries and free slip at the left hand side.

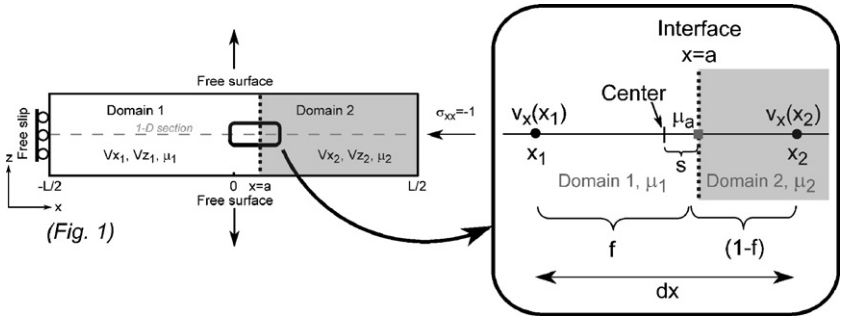

Fig. 2. Clip of 1D section showing two adjacent points x_1 and x_2, velocities $v_x(x_1)$ and $v_x(x_2)$, interface located at $x = a$, effective viscosity μ_a, factor f representing the fraction of μ_1 and s representing the shift from the center between x_1 and x_2.

$v_x^{\text{left}} = v_x(x = -L/2)$ and $v_x^{\text{right}} = v_x(x = L/2)$, then the velocity distribution for domain 1 and 2 is given by

$$v_x(x \le a) = \frac{v_x^a - v_x^{\text{left}}}{L/2 + a}(x - a) + v_x^a, \tag{13}$$

$$v_x(x \ge a) = \frac{v_x^{\text{right}} - v_x^a}{L/2 - a}(x - a) + v_x^a. \tag{14}$$

3.1.1.2. Stress distribution. The horizontal stress σ_{xx} in domain 1 and 2 can be computed from Eq. (12) and is given by

$$\sigma_{xx}(x \le a) = \frac{4\mu_1(v_x^a - v_x^{\text{left}})}{L/2 + a}, \tag{15}$$

$$\sigma_{xx}(x \ge a) = \frac{4\mu_2(v_x^{\text{right}} - v_x^a)}{L/2 - a}. \tag{16}$$

3.1.1.3. Velocity at the interface. Since $\sigma_{xx}(x \le a) = \sigma_{xx}(x \ge a)$, we can compute an expression for v_x^a from Eqs. (15) and (16):

$$v_x^a = \frac{v_x^{\text{left}}\mu_1(L - 2a) + v_x^{\text{right}}\mu_2(L + 2a)}{\mu_1(L - 2a) + \mu_2(L + 2a)}. \tag{17}$$

3.1.1.4. Constant stress. Substituting v_x^a into Eqs. (15) and (16) results in a stress, which is the same in the whole domain, σ_{xx} is

$$\sigma_{xx} = \frac{8(v_x^{\text{right}} - v_x^{\text{left}})\mu_2\mu_1}{\mu_1(L - 2a) + \mu_2(L + 2a)}. \tag{18}$$

3.1.2. Effective viscosity at the interface

In order to compare the analytical with the numerical results one needs to know the effective viscosity at the interface $x = a$, where a jump in viscosity occurs. Numerically, velocities and viscosities are only defined at discrete points in the domain. To derive the effective viscosity at $x = a$, we calculate the velocity at two adjacent points left (x_1) and right (x_2) of the interface (Fig. 2) using Eqs. (13) and (14):

$$v_x(x_1) = \frac{v_x^a - v_x^{\text{left}}}{L/2 + a}(x_1 - a) + v_x^a, \tag{19}$$

$$v_x(x_2) = \frac{v_x^{\text{right}} - v_x^a}{L/2 - a}(x_2 - a) + v_x^a. \tag{20}$$

Since σ_{xx} is constant and given by Eq. (18), we can calculate the effective viscosity μ_a at the interface a by substituting Eqs. (19), (20) and (17) in Eq. (12). Rearranging the equation yields

$$\mu_a = \frac{\mu_1\mu_2}{\mu_1((x_2 - a)/\mathrm{d}x) + \mu_2((-x_1 + a)/\mathrm{d}x)}, \tag{21}$$

where dx is the distance between x_1 and x_2. Eq. (21) can be reformulated by substituting $a = ((x_1 + x_2)/2) + s$, which is the location of the interface expressed by x_1 and x_2 and s representing the shift from the center within the two points x_1 and x_2 (Fig. 2). μ_a is then

$$\mu_a = \frac{\mu_1\mu_2}{\mu_1((((x_2 - x_1)/2) - s)/\mathrm{d}x) + \mu_2((((x_2 - x_1)/2) + s)/\mathrm{d}x)}. \tag{22}$$

Eq. (22) can be expressed by introducing a parameter f:

$$f = \frac{((x_1 - x_2)/2) + s}{\mathrm{d}x}, f \in [0, 1], \tag{23}$$

f represents the fraction of μ_1 on one side of the interface and $1 - f$ corresponds to the fraction of μ_2 on the other side of the interface between the two points x_1 and x_2. μ_a can then be rewritten as

$$\mu_a = \frac{\mu_1\mu_2}{\mu_1(1 - f) + \mu_2 f}. \tag{24}$$

3.1.2.1. Special case. If a is located in the center between x_1 and x_2 ($f = 0.5$) the effective viscosity simplifies to

$$\mu_a(f = 0.5) = \frac{2\mu_1\mu_2}{\mu_1 + \mu_2}. \tag{25}$$

This is the harmonic average of the two viscosities μ_1 and μ_2. f represents the weighting according to the fraction of μ_1 and μ_2 within x_1 and x_2, where the viscosity jump occurs.

3.2. Numerical solution

To solve the 1D problem outlined above numerically, we substitute the rheological equation in x-direction (Eq. (12)), into the force balance equation (Eq. (11)), which yields

$$4\frac{\partial}{\partial x}\left(\mu\frac{\partial v_x}{\partial x}\right) = 0, \tag{26}$$

subject to the boundary conditions $v_x(x = -(L/2)) = 0$ and $\sigma_{xx}(x = (L/2)) = -1$. Eq. (26) can be discretized with a standard, second order, finite difference scheme:

$$4\left(\mu^{i+(1/2)}\left(\frac{v_x^{i+1} - v_x^i}{\mathrm{d}x^2}\right) - \mu^{i-(1/2)}\left(\frac{v_x^i - v_x^{i-1}}{\mathrm{d}x^2}\right)\right) = 0, \tag{27}$$

where we assume constant grid-spacing dx. Velocities are defined at nodal points, whereas values of viscosity are defined at center points (Fig. 3(a) and (b)).

3.2.1. Different locations of the interface

Generally the following two cases can be distinguished:

(1) The interface between the two domains is located directly at a node (Fig. 3(a)). In this case, viscosities at all center points are unambiguously defined.
(2) The interface between the two domains is located in between two velocity points (Fig. 3(b)). In this case, the viscosity needs

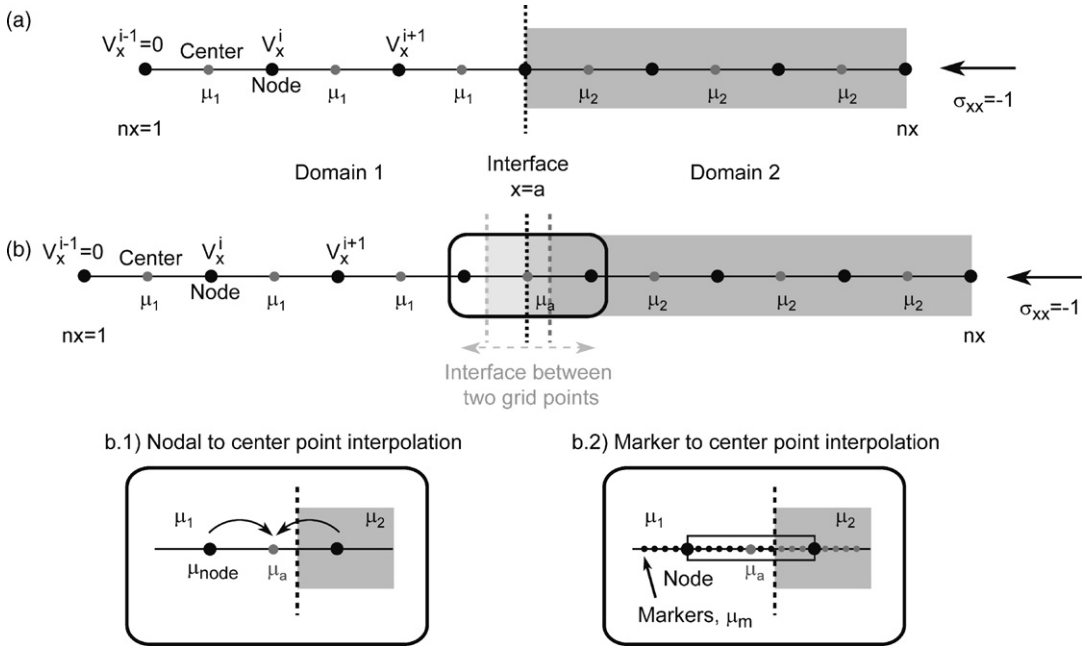

Fig. 3. Numerical scheme of 1D FD grid. Locations of velocity and viscosity are shown. (a) Case in which the interface is located at a node. (b) Case in which the interface is located in between two adjacent nodes.

to be effectively defined (μ_a). Through the analytical solution (Section 3.1.2), however, we can derive the effective viscosity value.

In case (1) the viscosities at all center points are clearly defined to have either the value μ_1 or μ_2. The numerical solution is identical with the analytical solution. In the more interesting case (2), an interpolation of the viscosity is required to obtain an appropriate viscosity value in a cell where two materials are present, with fractions of viscosity of values μ_1 and μ_2.

In Section 3.1.2 we derived the effective viscosity analytically (Eq. (24)). It is shown that this viscosity should ideally be a harmonic weighted average according to the fractions of either material. In numerical codes using Eulerian-type grids, volumetric fractions of different materials can be evaluated by using markers, which bear the different material properties, also known as marker-in-cell technique (Gerya and Yuen, 2003). While this is one way to solve this problem, in numerical codes, it is typically common to sample the material properties directly at either center or nodal points. The values are then projected to the points where they are required by interpolations. Therefore we evaluate the effect of viscosity averaging schemes on the accuracy of the numerical solutions. We compare numerical results with the analytical solution by applying interpolation methods such as simple averages and averages using markers to define material fractions and to locate the interface without knowing the exact location.

3.2.1.1. Simple averaging from nodal to center points. For simplicity, we restrict our analysis to cases in which viscosity is sampled at nodal points and then interpolated to center points using either arithmetic, geometric or harmonic averaging (Fig. 3(b.1)):

$$\mu_{\text{arith}} = \frac{\mu_1 + \mu_2}{2}, \tag{28}$$

$$\mu_{\text{geom}} = (\mu_1 \mu_2)^{0.5}, \tag{29}$$

$$\mu_{\text{harm}} = \frac{2\mu_1 \mu_2}{\mu_1 + \mu_2}. \tag{30}$$

Here, numerical simulations are performed using 10 grid points, $\mu_1 = 1$, $\mu_2 = 1000$, $L = 2$ and boundary conditions are $v_x(x = -(L/2)) = 0$ and $v_x(x = (L/2)) = -0.2$ so that $\sigma_{xx}(x = (L/2)) \approx -1$.

Numerical accuracies are derived by calculating the absolute error between the numerical and the analytical solution:

$$\text{error} = |v_{\text{num}} - v_{\text{ana}}|. \tag{31}$$

Numerical solutions of either averaging scheme (Eqs. (28)–(30)) are independent of the location of the interface, assuming that the interface only shifts between two fixed nodes (Fig. 3(b)). The analytical solution, on the other hand, yields different results for different locations of the interface. Comparing now the numerical and analytical solutions yields different accuracies for the three averaging schemes (Fig. 4). If the interface is exactly at the center point (Pos. 1) the harmonic average fits the analytical results perfectly. But if

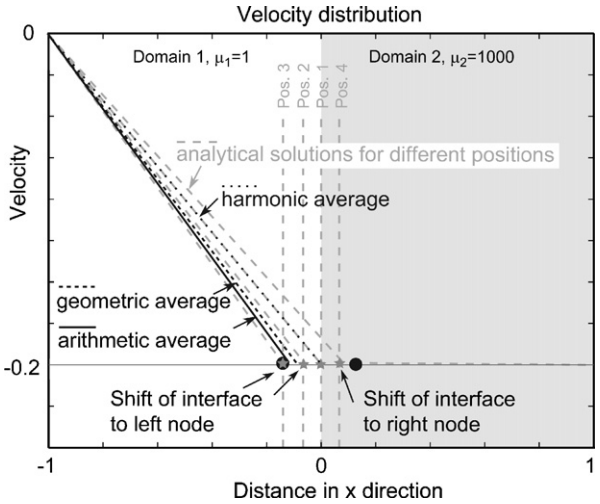

Fig. 4. Sketch of velocity distribution using simple averaging methods. Accuracies of different averaging methods depend on the location of the interface and on the viscosity contrast ($\geq$ or ≤ 1).

the interface is shifted to the left node (Pos. 2), then at a certain point the geometric average is better. If the interface is shifted even further so that it is located at the left node (Pos. 3), the arithmetic average yields best results. If the interface is shifted in the direction of the right node (Pos. 4), the accuracy order is the following: harmonic, geometric and then arithmetic average with decreasing accuracy. This implies that the accuracy is dependent on the location of the interface and in addition whether the viscosity jump is positive or negative.

3.2.1.2. Averaging from marker to center points. Here, numerical simulations are performed using $\mu_1 = 1$, $\mu_2 = 1000$, $L = 2$ and boundary conditions are $v_x(x = -(L/2)) = 0$ and $v_x(x = (L/2)) = -0.2$ such that $\sigma_{xx}(x = (L/2)) \approx -1$. Two different numbers of grid points ($nx = 10$ and $nx = 20$) and four different numbers of markers ($n_{\text{marker}} = 49, 99, 999$ and 1499) were tested (Fig. 3(b.2)).

A marker ratio is calculated which is similar to the parameter f introduced in Eq. (24):

$$f = \frac{n_{\text{marker}}(\mu_1)}{n_{\text{marker}}(\mu_1) + n_{\text{marker}}(\mu_2)}, \tag{32}$$

where the marker ratio is the number of markers bearing μ_1 ($n_{\text{marker}}(\mu_1)$) divided by the total amount of markers within one cell.

Further, the three averages (arithmetic, geometric and harmonic) are applied to the marker ratios in the following way:

$$\mu_{\text{marker-arith}} = \mu_1(f) + \mu_2(1-f), \tag{33}$$

$$\mu_{\text{marker-geom}} = \mu_1^f \mu_2^{1-f}, \tag{34}$$

$$\mu_{\text{marker-harm}} = \frac{\mu_1 \mu_2}{\mu_1(1-f) + \mu_2(f)}. \tag{35}$$

Comparison between the numerical and analytical results show that the harmonic marker ratio average yields the best results which is not surprising given the resemblance of Eq. (24) and Eq. (35). Fig. 5 shows that with increasing number of markers the accuracy of the numerical solution increases for the harmonic marker ratio average but remains poor for the arithmetic and geometric marker ratio averages. Further tests show that the errors slightly depend on the position of the interface and are best for an interface located in the center but the relative accuracies of the harmonic, geometric and arithmetic marker ratio averages remain the same.

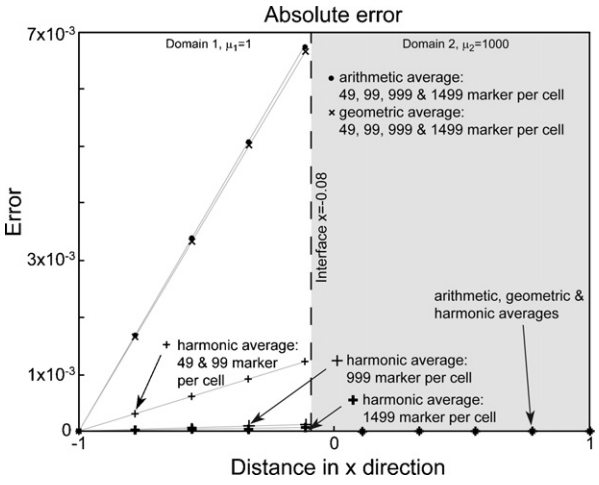

Fig. 5. Absolute error between numerical and analytical solution. Numerical solutions are calculated by using four different numbers of markers $n_{\text{marker}} = 49, 99, 999, 1499$. Number of gird points is $nx = 10$ and the interface is shifted by -0.08. By an increasing amount of markers only results using a harmonic average improve.

Tests with a higher resolution ($nx = 20$) indicate a slightly smaller error than results produced with $nx = 10$, but this improvement is relatively small for the already good results of the harmonic marker ratio average.

The 1D analysis thus demonstrates that discontinuities in material properties require careful tuning of the viscosity within the cell where material properties change. If significant jumps in viscosity occur between adjacent nodal points, harmonic marker ratio averaging is to be preferred. Applying the findings of the 1D analysis in 2D, however, shows that the 2D FD formulations and the viscosity averaging methods are more complicated to understand. Part of the problem is that in the 2D numerical formulation, viscosity needs to be defined not only at center points but also at nodal points. One could speculate that a harmonic marker ratio averaging, ones from markers to center points and once from markers to nodal points, should yield the best results in 2D. As it will be shown next this is not entirely the case. Thus the connection between the 1D analysis and the 2D numerical results is not straightforward.

4. 2D governing equations and numerical methods

4.1. 2D governing equations

The Stokes equations (Eqs. (1)–(5)) in 2D are

$$\frac{\partial v_x}{\partial x} + \frac{\partial v_z}{\partial z} = 0, \tag{36}$$

$$-\frac{\partial P}{\partial x} + 2\frac{\partial}{\partial x}\left(\mu \frac{\partial v_x}{\partial x}\right) + \frac{\partial}{\partial z}\left(\mu\left(\frac{\partial v_x}{\partial z} + \frac{\partial v_z}{\partial x}\right)\right) = 0, \tag{37}$$

$$-\frac{\partial P}{\partial z} + 2\frac{\partial}{\partial z}\left(\mu \frac{\partial v_z}{\partial z}\right) + \frac{\partial}{\partial x}\left(\mu\left(\frac{\partial v_x}{\partial z} + \frac{\partial v_z}{\partial x}\right)\right) = \rho g. \tag{38}$$

Eq. (36) represents conservation of mass, Eqs. (37) and (38) represent conservation of momentum in x- and in z-direction.

In presence of highly varying viscosity, the Stokes solver is critical for accurate results. Therefore, accuracy tests for pressure and velocity solutions are performed for three different FDM and an FEM using different arrangements of the elements. These are

(1) Staggered grid velocity–pressure FDM.
(2) Stream function FDM.
(3) Rotated staggered grid velocity–pressure FDM.
(4) Unstructured velocity–pressure FEM.

The staggered grid velocity–pressure FDM is commonly used to solve the Stokes equations (e.g. Gerya and Yuen, 2003; Katz et al., 2007). The stream function FDM introduces an additional parameter: the stream function Ψ. The difference between the stream function value at any two points gives volumetric flow rate (flux) between the points. It is useful when studying fluid dynamics since the velocity field can directly be calculated from the stream function (as is often done in mantle convection codes, Schmeling and Jacoby, 1981). The rotated staggered grid FDM was first introduced by Saenger et al. (2000). Advantages of the rotated staggered grid are that viscosity is defined only in the center of a cell and that velocities are calculated at the same nodal points.

Accuracy of the numerical methods is compared using two different types of tests. One is a 2D analytical solution for the pressure distribution around an inclusion embedded in a viscous matrix developed by Schmid and Podladchikov (2003). A second test was

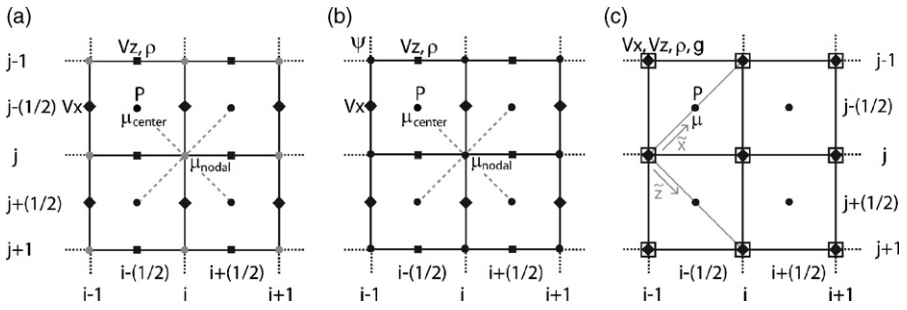

Fig. 6. Numerical grid for the three FDM employed in this work. Displayed are four cells for each method. Locations where pressure, velocities, viscosity and other parameters are defined are shown. (a) Staggered grid FDM. Four adjoining center point-viscosities are interpolated to one nodal point-viscosity. (b) Stream function FDM with nodal point- and center point-viscosities. Interpolation is done the same way as for (a). (c) Rotated staggered grid FDM.

performed for the analytical solution of Rayleigh–Taylor instabilities (Biot, 1961; Biot and Odé, 1965).

The numerical codes have been developed for the purpose of this work. The implementation was done in MATLAB®, and direct solvers have been applied in all cases. Since the focus here is on the accuracy of the methods rather than on the formulation itself we keep the technical discussion of each of the methods brief.

4.1.1. Staggered grid velocity–pressure finite difference method

The 2D Stokes equations are solved on a staggered grid (e.g. Gerya and Yuen, 2003), where pressure and both velocities in x- and z-direction are discretized at physically different positions on the grid (Fig. 6(a)). Viscosity is defined in the center and at nodal points of a cell. Density is defined between two nodal points at the position of the velocity in z-direction.

Examples of the discretizations of Eq. (36) and the second part of Eq. (37) ($2(\partial/\partial x)(\mu(\partial v_x/\partial x))$) are

$$\frac{v_x^{i,j-(1/2)} - v_x^{i-1,j-(1/2)}}{\mathrm{d}x} + \frac{v_z^{i-(1/2),j} - v_z^{i-(1/2),j-1}}{\mathrm{d}z} = 0,$$

and

$$2\frac{\partial}{\partial x}\left(\mu\frac{\partial v_x}{\partial x}\right) = 2\left(\frac{\mu^{i+(1/2),j-(1/2)}(v_x^{i+1,j-(1/2)} - v_x^{i,j-(1/2)})}{\mathrm{d}x^2}\right) - 2\left(\frac{\mu^{i-(1/2),j-(1/2)}(v_x^{i,j-(1/2)} - v_x^{i-1,j-(1/2)})}{\mathrm{d}x^2}\right). \tag{39}$$

Discretization of the Stokes equations (Eqs. (37) and (38)) requires the viscosity to be defined at both nodal and center points of a control volume. For the discretization of the derivative of the normal stress component ($(\partial\sigma_{xx}/\partial x)$, $(\partial\sigma_{zz}/\partial z)$), as shown, e.g. in Eq. (39), viscosity has to be defined in the center of the control volume. For the discretization of the derivative of the shear stress component ($(\partial\sigma_{xz}/\partial x)$, $(\partial\sigma_{xz}/\partial z)$) viscosity needs to be defined at nodal points (this can be derived similarly).

It will be shown later that in the variable viscosity case, the manner in which viscosities are defined at center and nodal points is important for the overall accuracy of the solution. Typically, viscosity is defined at center points and then interpolated to nodal points. Other cases are described later and discussed in details. Pressure is always located at the center of a cell.

4.1.2. Stream function finite difference method

For the stream function finite difference method (e.g. Tannehill et al., 1997; Fletcher, 1991) the Stokes equations are simplified by eliminating pressure P, and introducing a stream function Ψ:

(a) Pressure is eliminated by taking the derivative of Eq. (37) in z-direction and subtracting the x-derivative of Eq. (38):

$$-4\frac{\partial^2}{\partial x\partial z}\left(\mu\frac{\partial v_z}{\partial z}\right) + \frac{\partial^2}{\partial z^2}\left(\mu\left(\frac{\partial v_x}{\partial z} + \frac{\partial v_z}{\partial x}\right)\right) - \frac{\partial^2}{\partial x^2}\left(\mu\left(\frac{\partial v_x}{\partial z} + \frac{\partial v_z}{\partial x}\right)\right) = -\frac{\partial}{\partial x}\rho g. \tag{40}$$

(b) The stream function Ψ is introduced:

$$v_x = \frac{\partial\Psi}{\partial z}, \qquad v_z = -\frac{\partial\Psi}{\partial x}. \tag{41}$$

(c) Substituting Eq. (41) into Eq. (40) results in a fourth order partial differential equation for Ψ:

$$4\frac{\partial^2}{\partial x\partial z}\left(\mu\frac{\partial^2\psi}{\partial x\partial z}\right) + \frac{\partial^2}{\partial z^2}\left(\mu\left(\frac{\partial^2\psi}{\partial z^2} - \frac{\partial^2\psi}{\partial x^2}\right)\right) - \frac{\partial^2}{\partial x^2}\left(\mu\left(\frac{\partial^2\psi}{\partial z^2} - \frac{\partial^2\psi}{\partial x^2}\right)\right) = -\frac{\partial}{\partial x}\rho g. \tag{42}$$

The advantages of the stream function approach are that it satisfies the incompressibility condition exactly and that it reduces the number of variables (and equations) from three to one. The disadvantage is that fourth order derivatives occur (rather than merely second order as in the velocity–pressure formulation). This makes the implementation of boundary conditions cumbersome. Moreover the stream function approach is more difficult to extend to 3D (Fletcher, 1991; Tannehill et al., 1997).

Eq. (42) is discretized at the nodal points of a staggered numerical grid. Material properties (viscosity and density) are defined at the center points of the cell (Fig. 6(b)). For discretization of differential operators of second order in the same direction (e.g. $(\partial^2/\partial x^2)(\partial^2/\partial x^2)$ or $(\partial^2/\partial x^2)(\partial^2/\partial z^2)$) viscosity needs to be defined at the nodal points. Discretization of second order operators in two directions (e.g. $(\partial^2/\partial x\partial z)(\partial^2/\partial x\partial z)$) requires the viscosity to be defined in the center of the cell. This is shown for the discretization of the part $((\partial^2/\partial z^2)(\mu(\partial^2\Psi/\partial z^2)))$ of Eq. (42), which requires the viscosity at nodal points:

$$\frac{\partial^2}{\partial z^2}\left(\mu\left(\frac{\partial^2\Psi}{\partial z^2}\right)\right) = \frac{\mu^{i,j+1}}{\mathrm{d}z^2}\left(\frac{\Psi^{i,j+2} - 2\Psi^{i,j+1} + \Psi^{i,j}}{\mathrm{d}z^2}\right) - \frac{2\mu^{i,j}}{\mathrm{d}z^2}\left(\frac{\Psi^{i,j+1} - 2\Psi^{i,j} + \Psi^{i,j-1}}{\mathrm{d}z^2}\right) + \frac{\mu^{i,j-1}}{\mathrm{d}z^2}\left(\frac{\Psi^{i,j} - 2\Psi^{i,j-1} + \Psi^{i,j-2}}{\mathrm{d}z^2}\right). \tag{43}$$

Therefore viscosity is interpolated from center to nodal points using the same interpolation methods as in the case of the staggered grid FDM.

Once the governing equations are solved for Ψ, v_x and v_z can be computed through Eq. (41). Pressure is computed by using Eq. (37) or (38). Pressure and velocities v_x and v_z, finally, are located at the same positions as for the staggered grid FDM (Fig. 6(a) and (b)). Density is located at the position of the velocity in z-direction.

4.1.3. Rotated staggered grid velocity–pressure finite difference method

Both the staggered grid and the stream function formulation require viscosity to be defined at two different locations, which introduces additional problems such as how viscosity should be interpolated from one point to the other. It therefore seems advantageous to have a method in which material properties are defined at a single location only. One such method is the rotated staggered grid velocity–pressure formulation, first developed by Saenger et al. (2000) in the context of seismic wave propagation in strongly heterogeneous media. The main difference of this method to the normal staggered grid method is the rotation of the control volume by 45°. Directions of spatial derivatives are performed along the $\tilde{x}$- and $\tilde{z}$-axes (Fig. 6(c)). For example for Eq. (36) this is

$$\frac{1}{2}\left(\frac{\left(v_x^{i+1,j+1}-v_x^{i,j+1}\right)}{\mathrm{d}x}+\frac{\left(v_x^{i+1,j}-v_x^{i,j}\right)}{\mathrm{d}x}\right)+\frac{1}{2}\left(\frac{\left(v_z^{i+1,j+1}-v_z^{i+1,j}\right)}{\mathrm{d}z}+\frac{\left(v_z^{i,j+1}-v_z^{i,j}\right)}{\mathrm{d}z}\right)=0, \tag{44}$$

and for the part $(\partial/\partial z)(\mu(\partial v_z/\partial x))$ of Eq. (37) this is

$$\begin{aligned}\frac{\partial}{\partial z}\left(\mu\left(\frac{\partial v_z}{\partial x}\right)\right) &= \frac{\mu^{i+(1/2),j+(1/2)}}{4}\left(\frac{v_z^{i+1,j+1}-v_z^{i,j+1}+v_z^{i+1,j}-v_z^{i,j}}{\mathrm{d}x\,\mathrm{d}z}\right)\\ &-\frac{\mu^{i+(1/2),j-(1/2)}}{4}\left(\frac{v_z^{i+1,j}-v_z^{i,j}+v_z^{i+1,j-1}-v_z^{i,j-1}}{\mathrm{d}x\,\mathrm{d}z}\right)\\ &+\frac{\mu^{i-(1/2),j+(1/2)}}{4}\left(\frac{v_z^{i,j+1}-v_z^{i-1,j+1}+v_z^{i,j}-v_z^{i-1,j}}{\mathrm{d}x\,\mathrm{d}z}\right)\\ &-\frac{\mu^{i-(1/2),j-(1/2)}}{4}\left(\frac{v_z^{i,j}-v_z^{i-1,j}+v_z^{i,j-1}-v_z^{i-1,j-1}}{\mathrm{d}x\,\mathrm{d}z}\right).\end{aligned} \tag{45}$$

See Saenger et al. (2000) for more details on differential operators using the rotated staggered grid.

The main advantage of the present method is that viscosity is defined at center points only. Velocities are located at nodal points and pressure is located at center points. Densities are located at nodal points. A problem, however, is the appearance of a checkerboard pressure (Saenger and Bohlen, 2004). A possible remedy, which was applied here, is to average pressure arithmetically in the space domain over four neighboring points.

4.1.4. Unstructured finite element method

The FD discretization techniques outlined above assumes pressure to be continuous. In the case of strongly varying viscosity, this is not the case and one could thus expect that methodologies with discontinuous pressures yield better results. In order to verify this, we also employed an unstructured FE code for the tests described here. Solving the incompressible Stokes equations with a FE approach is slightly tricky, since the employed elements should satisfy the *inf–sup* stability condition (Cuvelier et al., 1986; Elman et al., 2005). The widely used $Q_1 - P_0$ element (linear shape functions for velocity and constant shape functions for pressure) does not satisfy this condition and more complex elements have to be employed instead. Here, we use the FE code MILAMIN (see Dabrowski et al., 2008, for code and detailed description) that employs triangular elements with *inf–sup* stable $Q_2 - P_1$ shape functions.

Since the code uses isoparametric elements, viscosity is sampled at integration points (6 for the cases shown here). For simple setups, it is possible to use a mesh generator that creates a grid, which satisfies internal phase boundaries in such a way that each element has well-defined (and constant) viscosities. In more complex marker-in-cell models, situations may occur in which different integration points in the same element have different viscosities. Since pressure is assumed to vary in a linear manner within each element, strong jumps in viscosity might result in numerical artefacts. One can than thus either (1) leave the viscosity as it is, i.e. directly sample at integration points or (2) average the viscosity at an element-level using, e.g. arithmetic or harmonic averages. It will be demonstrated below that the accuracy of the solution strongly depends on the method of choice.

5. Viscosity interpolation methods for finite difference methods

Discretization of the Stokes equations for the staggered grid and stream function FDM requires viscosity to be defined at both nodal and center points of a control volume (Fig. 6(a) and (b)). The 1D analytical solution (Section 3) showed that an effective viscosity should be calculated if an interface intersects a cell. Markers can be used to evaluate a more exact location of an interface intersecting a cell (marker-in-cell method employed in Gerya and Yuen, 2003; Weinberg and Schmeling, 1992; Tackley and King, 2003, to define material properties). In this case the marker ratio (Eq. (32)) for each cell is calculated. In the numerical algorithms viscosity is defined in different ways. The different interpolation methods, nomenclature and general signature are summarized in Fig. 7. Interpolations are performed with and without markers. Some combinations ((b)–(d)) are compared with the reference-methods (a). The reference-methods are

- *Without markers*: directly defined viscosities at center points and simply interpolated from center to nodal points (center2node).
- *With markers*: combining the interpolation from markers to center points (marker2center) and the interpolation from center to nodal points (center2node).

For each of the used interpolation methods one of the three averages is applied:

$$\text{Arithmetic average}: \quad A_n = \frac{a_1 + a_2 + a_3 + \cdots + a_n}{n},$$

$$\text{Geometric average}: \quad G_n = \sqrt[n]{a_1 a_2 \cdots a_n},$$

$$\text{Harmonic average}: \quad H_n = \frac{n}{(1/a_1) + (1/a_2) + \cdots + (1/a_n)},$$

where $H_n \le G_n \le A_n$ is always valid. This is the general formulation. When using markers the equations can be expressed by using the marker ratios (Eqs. (33)–(35)).

Note that the rotated staggered grid FDM does not requires viscosity interpolation. However, markers were implemented for an interpolation from markers to center points for comparison and in cases where an interface has to be resolved within a cell. The FEM

Viscosity interpolation methods for FDM

The following interpolation methods are combined in differnent ways. One method is chosen for the viscosity at the center point (μ_{center}) and one for the viscosity at the nodal point (μ_{node}). The combinations of *marker2center* for μ_{center} and *center2node* for μ_{node} so as without markers *directly-defined* for μ_{center} and *center2node* for μ_{node} serve as a reference ((a) Reference). Certain combinations are very similar to the reference interpolation methods. These combinations are aligned with the reference interpolation methods.

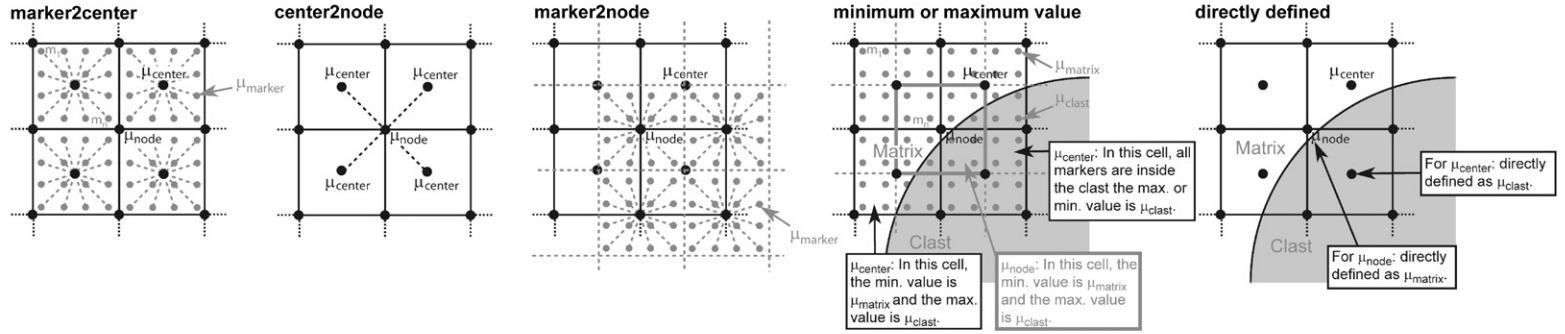

a) Reference				d) 2-times-markers				b) Direct/marker				c) Minimum/maximum			
Symbol	Nomenclature CENTER-NODE	Interpolation method Center	Node	Symbol	Nomenclature CENTER-NODE	Interpolation method Center	Node	Symbol	Nomenclature CENTER-NODE	Interpolation method Center	Node	Symbol	Nomenclature (C-N)	Interpolation method Center	Node
•	ARITH	directly defined	center2node					•	DIRECT-ARITH	directly defined	marker2node				
x	GEOM	directly defined	center2node												
+	HARM	directly defined	center2node					✚	DIRECT-HARM	directly defined	marker2node				
○	ARITH-ARITH	marker2center	center2node	○	ARITH-HARM	marker2center	marker2node								
	[1]ARITH-GEOM	marker2center	center2node												
☆	ARITH-HARM	marker2center	center2node									★	MAX-MIN	max. value	min. value
	[1]GEOM-ARITH	marker2center	center2node												
△	GEOM-GEOM	marker2center	center2node	△	GEOM-GEOM	marker2center	marker2node								
✳	GEOM-HARM	marker2center	center2node	✳	GEOM-HARM	marker2center	marker2node								
▽	HARM-ARITH	marker2center	center2node									▼	MIN-MAX	min. value	max. value
	[1]HARM-GEOM	marker2center	center2node												
□	HARM-HARM	marker2center	center2node	□	HARM-HARM	marker2center	marker2node					■	MIN-MIN	min. value	min. value
								○	ARITH-DIRECT	marker2center	directly defined				
								■	HARM-DIRECT	marker2center	directly defined				

Different FD methods

——— Staggered grid FDM – – – – – Stream funtion FDM ····· Rotated staggered grid FDM

[1] All combinations are systematically tested with the staggered grid FDM (section 7.1.2), but only selections of the combinations with a given symbol are used for further comparisons. For systematic testing of the staggered grid FDM using the reference-methods (a) different symbols and line styles are used, which are described in the corresponding *Fig. 11*.

Fig. 7. Schematic description of the viscosity interpolation methods, nomenclature and signatures used for FDM.

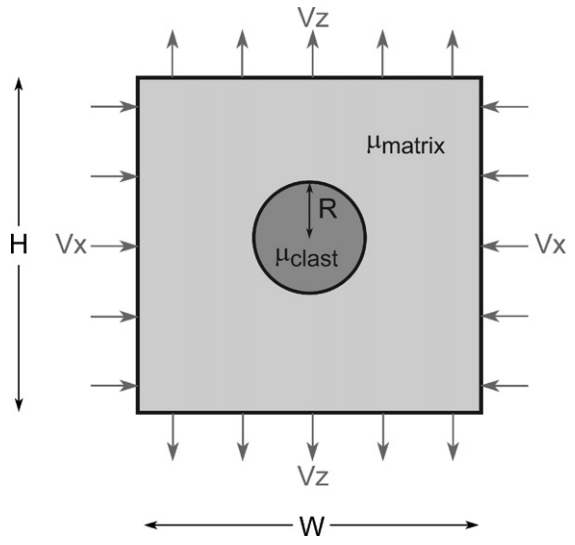

Fig. 8. Initial model setting of circular inclusion test showing pure shear boundary conditions and other parameters described in the text.

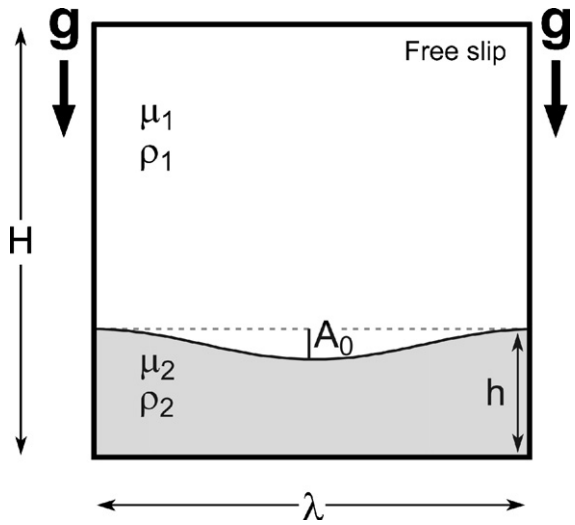

Fig. 9. Initial model setting for RT instability test showing free slip boundary conditions, gravity g and other parameters described in the text.

requires no interpolation if a perfectly fitted mesh is employed. In some other cases, an averaged viscosity value for the element was computed. A detailed description of the different FE mesh generation and averaging techniques is given in Section 7.1.4.

6. Model setups

The accuracy of the three different FD formulations was compared to analytical solutions in two different cases: (1) a circular inclusion test and (2) a Rayleigh–Taylor instability test. The FEM results were only compared with the circular inclusion test.

6.1. Circular inclusion test

Numerical simulations were performed for a homogeneous circular inclusion embedded in a homogeneous matrix of different viscosity (Fig. 8). Unless mentioned otherwise, the initial setup of the model is a strong inclusion in a surrounding weak matrix using a non-dimensionalized viscosity contrast between inclusion (clast) and matrix of 1000. All physical model parameters are non-dimensionalized by using the characteristic scales given in Table 1.

Boundary conditions are pure shear background strain rate: the analytical solution of the velocity of Schmid and Podladchikov (2003) is implemented at all four boundaries. The applied velocity boundary conditions are compressive in horizontal and extensional in vertical directions. Calculations are done for a static problem with a single time step.

Table 1
All physical parameters for the model of a circular inclusion in a viscous matrix have been non-dimensionalized by the characteristic scales

	Value
Characteristic scales	
Char. length scale	$L_c = H$
Char. time scale	$t_c = 1/\dot{\varepsilon}_{BG}$
Char. viscosity	$\mu_c = \mu_{matrix}$
Model parameters	
Viscosity matrix (embedding material)	$\mu_{matrix} = 1$
Viscosity circular inclusion	$\mu_{clast} = 1000$ (strong inclusion)
	$\mu_{clast} = 0.001$ (weak inclusion)
Width of domain	$W = 2$
Height of domain	$H = 2$
Radius of circular inclusion	$R = 0.1$
Strain rate	$\dot{\varepsilon}_{BG} = 1$

6.2. Rayleigh–Taylor instability test

Rayleigh–Taylor (RT) instabilities occur due to the fact that in case of a density inversion the lighter material tends to go on top of heavy material (e.g. Biot and Odé, 1965; Burg et al., 2004).

The simplest form is a test using two horizontal layers with a heavy top layer overlying a lighter bottom layer and an initial perturbation of one wavelength, which drives the system without any background driving force (Fig. 9). The analytical solution and the controlling parameters are discussed by different authors (e.g. Biot and Odé, 1965; Whitehead, 1988). Here, their results are employed to test accuracy of the different numerical schemes.

A layer of thickness h, density ρ_2, and viscosity μ_2 underlies a layer of thickness $H - h$, density ρ_1, and viscosity μ_1. All physical model parameters are non-dimensionalized by using the characteristic scales given in Table 2.

Boundary conditions are free slip at all four sides of the domain. Calculations are done for a static problem with a single time step. Simulations are performed for different dimensionless wavelengths ($\lambda = 0.5$–6).

Table 2
All physical parameters for the RT instability models are non-dimensionalized by using the characteristic scales

	Value
Characteristic scales	
Char. length scale	$L_c = H$
Char. viscosity	$\mu_c = \mu_2$
Char. stress	$\sigma_c = \Delta\rho g H$
Model parameters	
Viscosity top layer	$\mu_1 = 1000$
Viscosity bottom layer	$\mu_2 = 1$
Width of domain	$W = \lambda$
Height of domain	$H = 1$
Density of top layer	$\rho_1 = 1$
Density of bottom layer	$\rho_2 = 2$
Gravity	$g = 10$
Amplitude	$A_0 = 0.001H$

7. Results

7.1. Circular inclusion test

7.1.1. 2D pressure distribution

In Schmid and Podladchikov (2003) a 2D analytical solution is derived for the setup given in Section 6.1. Pressure is defined throughout the whole domain and is directly used to evaluate the accuracy of the numerical schemes. For the previously described pure shear boundary conditions, the analytical solution has zero pressure inside the strong clast and highest and lowest pressures directly at the clast–matrix boundary (Fig. 10(a)).

Fig. 10(b) shows the numerically computed pressure distribution using the staggered grid FDM, with arithmetic viscosity averaging (center2node). Differences in maximum pressure of up to 244% occur versus the analytical solution. If, on the other hand, a 20×20-marker-based harmonic average from markers to center points and then a harmonic average from center to nodal points is used (reference interpolation method: HARM–HARM, Fig. 10(c)), the accuracy of the method increases and the error is reduced to 11%. This large improvement is mainly due to the averaging type and only secondary due to the use of markers (Section 7.1.2).

For all methods, the highest errors occur close to the material interface (at the boundary between clast and matrix). For the staggered grid (Fig. 10(b) and (c)) and the stream function FDM (Fig. 10(d)) an oscillating pressure field can be observed. Large positive and large negative pressure values alternate along the clast–matrix boundary.

Pressure calculated with the rotated staggered grid finite difference method (Fig. 10(e)) has a checkerboard pressure at the clast–matrix boundary, if the pressure is unfiltered. Pressure-averaging reduces the error, although some oscillations remain (Fig. 10(e)).

7.1.2. Effect of viscosity interpolation for the staggered grid FDM (reference interpolation methods)

The influence of the viscosity interpolation methods is systematically tested using the reference interpolation methods with and without markers. Since the results of the three numerical methods are very similar, only the results for staggered grid FDM are presented here.

The error is computed as the root mean square error, which is

$$\text{RMS error} = \sqrt{\frac{\int_A (X_{\text{num}} - X_{\text{ana}})^2 \, \mathrm{d}A}{\int_A (X_{\text{ana}})^2 \, \mathrm{d}A}}, \tag{46}$$

where X_{num} indicates numerically computed values and X_{ana} the analytical solution at the same location, A is the total area of the domain.

The RMS errors of the pressure and velocity versus numerical resolution using the reference interpolation methods are shown in Fig. 11. The error generally decreases with increasing resolution. The unstable behavior (alternating larger and smaller errors) of the curves is a result of the numerical discretization of the inclusion boundaries. With an equally spaced rectangular grid a circular inclusion has a stair-shaped boundary. With increasing resolution, the clast is filled with an incremental number of cells. During this process the stair-shaped boundary of the clast varies slightly. Some clast shapes improve the accuracy of the pressure solution.

The results of the pressure error (Fig. 11(a)) and the velocity error (Fig. 11(b)) show an opposite behavior of the grouping related to the viscosity interpolation method. The pressure models using harmonic average from center to nodal points show smallest errors (second interpolation step, solid-black lines) while the velocity models using harmonic average from marker to center points (first interpolation step, crosses) have more accurate results. Additional results produced by FEM with perfectly fitting elements around the clast have results that are more than one to two orders of magnitude better than for the staggered grid FDM. For pressure and velocity, the weight of the markers is too small to improve the results significantly. When an inappropriate interpolation method such as arithmetically (ARITH) averaged center2node interpolation was chosen (dotted lines), then interpolation methods with and without markers show all bad accuracies for the pressure error. The same is valid for the velocity models, a harmonically (HARM) averaged center2node interpolation without markers shows as good results as methods using markers. Smallest errors are obtained for a marker-based method in which viscosity is harmonically averaged from markers to center points and from center to nodal points. For pressure, geometrically averaged viscosities from marker to center and harmonic averages from center to nodal points yield more accurate results for higher resolutions, although the difference is small.

7.1.3. 2-Times-marker, direct/marker and minimum/maximum viscosity interpolation methods

A selection of other combinations of different viscosity interpolation methods (Fig. 7) are compared with the results shown of the staggered grid FDM (Fig. 11). These are the 2-times-marker, direct/marker and minimum/maximum interpolation methods. Results are plotted in the frame of the results of the staggered grid FDM (Fig. 12). One could expect that a double marker interpolation, once from marker to center points and once from center to nodal points, would represent the findings from the 1D analysis best. We showed that a harmonically averaged marker interpolation represents the 1D analytical solution almost perfectly. Thus a double harmonic marker interpolation (2-times-marker) should yield best results, which is not the case for the pressure, but only for the velocity solution. A possible cause for this is that the 1D solution is only solved for velocity. In addition, pressure is only a first order derivative compared to the second derivative of the velocity. For three other averaging combinations (ARITH–HARM, GEOM–GEOM and GEOM–HARM) the improvements are very small.

Also the direct/marker and the minimum/maximum interpolation methods are all within the given range of the error calculated by the reference interpolation methods. Interesting is the fact that some interpolation methods correlate very well with the reference methods. For example, the simple harmonically averaged viscosities from center to nodal points (HARM reference solution) and the solution using a directly sampled viscosity for the center points and a harmonic averaged marker to nodal points interpolation (DIRECT-HARM direct/marker solution) differ only very little (Fig. 12(b)). The only difference is that for the latter markers are used for the interpolation, which again shows that markers have no significant effect on the overall accuracy. The opposite behavior of the ARITH-DIRECT and HARM-DIRECT for pressure and velocity solutions leads to the assumption, that pressure solutions prefer to have smooth viscosity steps between center and nodal points while for the velocity solutions large jumps at the nodal points are preferred. The minimum/maximum interpolation methods show that the ARITH–HARM reference solution correlates very well with the MAX-MIN solution (Fig. 12(c)) which might be related to the fact that the arithmetic averages have the largest values and the harmonic averages the smallest. But the HARM–HARM reference solution and the MIN-MIN solution do not correlate at all. The discretized shape of the clast is strongly affected by the MIN-MIN solution and creates probably a too small clast. The MIN-MIN solution does not represent the same as the HARM–HARM reference or the HARM–HARM 2-times-marker solution.

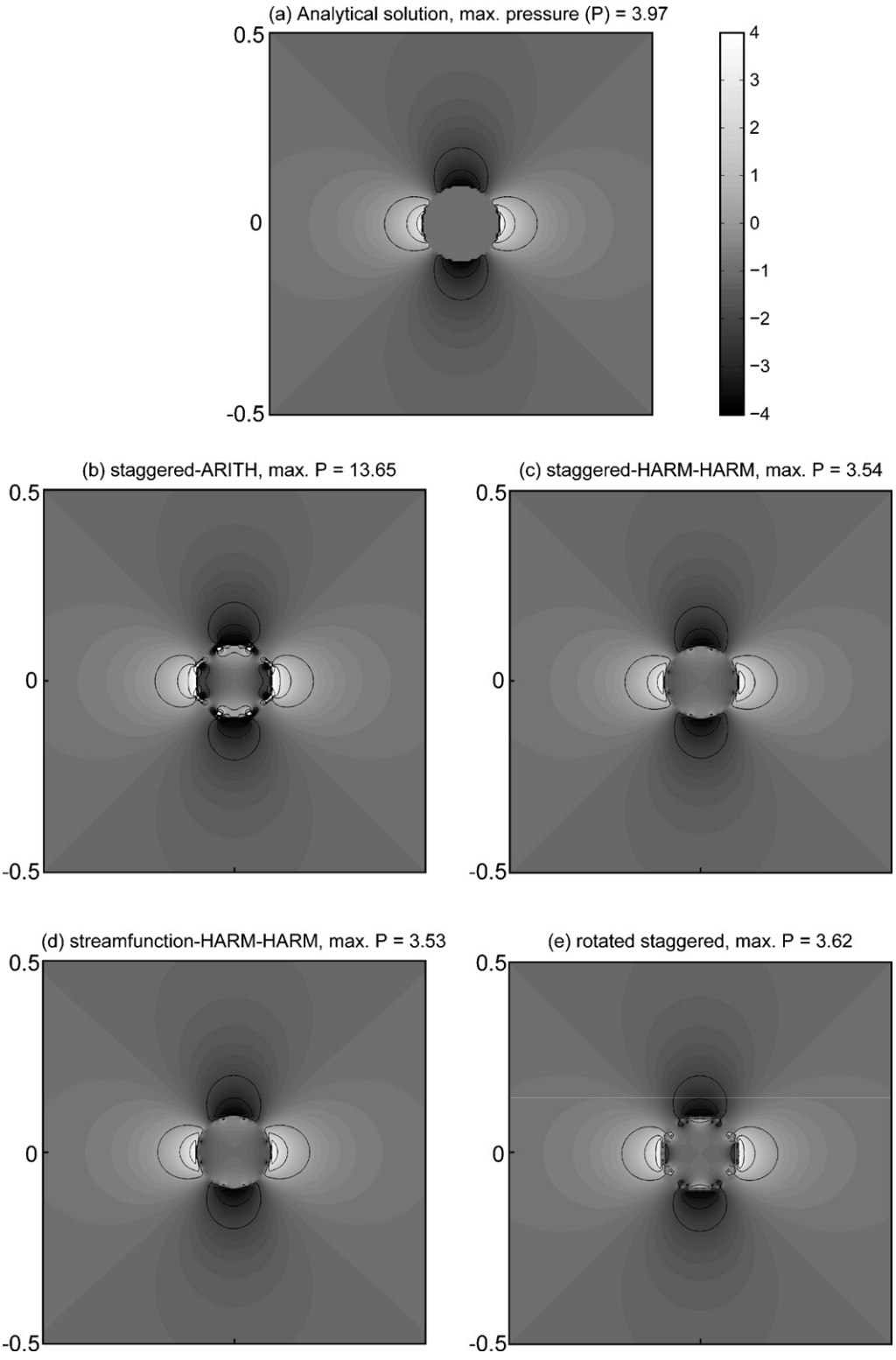

Fig. 10. 2D pressure fields using a viscosity contrast of $\mu_{clast}/\mu_{matrix} = 1000$ and a resolution of 280 × 280 grid points. Contours are at −4, −3, −2, −1, 1, 2, 3, 4. (a) Analytical solution. (b–e) Numerical solutions using reference interpolation methods. (b) Staggered grid FDM, ARITH-interpolation, no markers. (c) Staggered grid FDM, HARM–HARM interpolation, 20 × 20 markers per cell. (d) Stream function FDM, HARM–HARM interpolation, 20 × 20 markers per cell. (e) Rotated staggered grid FDM. See text for discussion.

7.1.4. Comparison of numerical methods

To visualize the accuracy of the pressure and the velocity solution of the different numerical techniques the RMS error (Eq. (46)) is plotted versus resolution for some representative cases. The accuracy of the pressure solution (Fig. 13) is typically less than for velocity solution. The errors of the velocity compared to the pressure solution are almost one order of magnitude less for the staggered grid and stream function FDM for the corresponding viscosity interpolation methods.

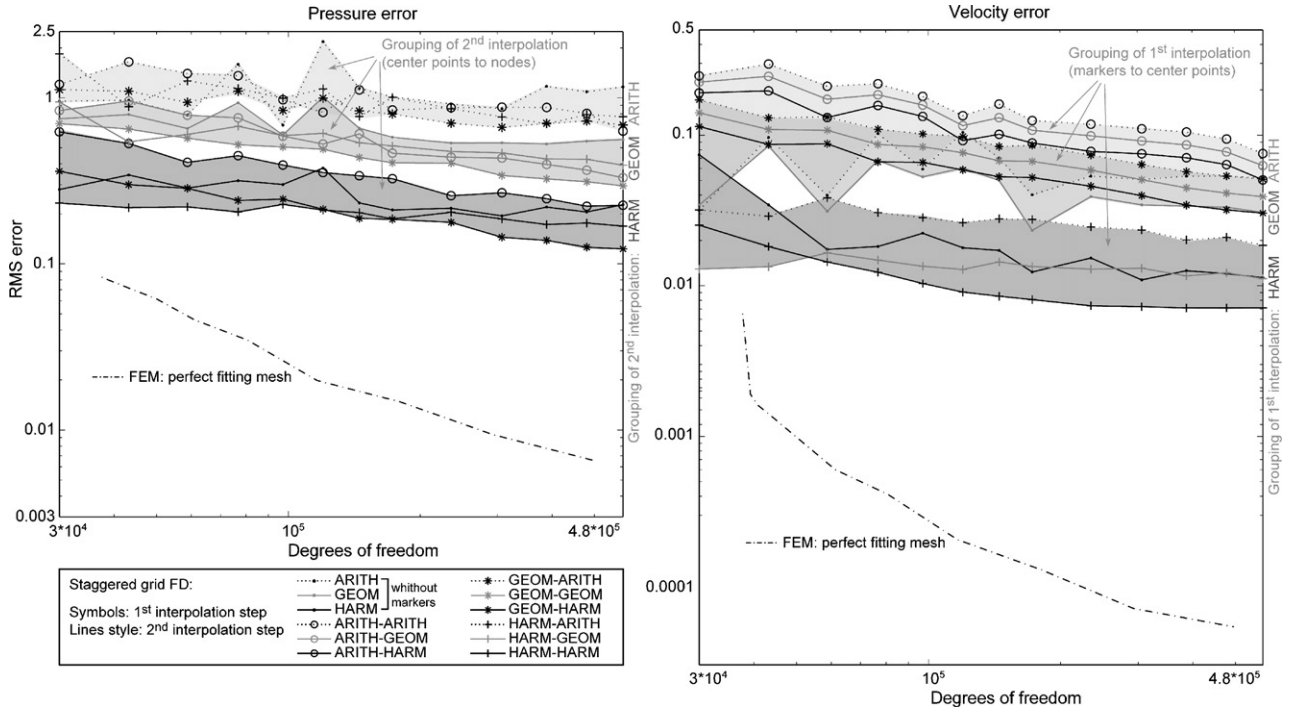

Fig. 11. RMS error of pressure and velocity as a function of resolution for different viscosity interpolation methods (circular inclusion test). Staggered grid FDM and an FEM with perfectly fitting elements around the clast are displayed. For the staggered grid FDM only reference interpolation methods (Fig. 7) are applied. For this figure different line and symbol styles are used than defined in Fig. 7. Most cases employ markers in which viscosity is first interpolated from markers to center points (marker2center), followed by a second interpolation from center to nodal points (center2node). In cases where no markers are employed (viscosity directly sampled at center points) only the second interpolation step is applied. FEM-results show more than one order of magnitude smaller pressure- and velocity errors. For the staggered grid FDM smallest pressure errors (a) occur for HARM averaging from center to nodal points (grouping due to second interpolation step) and smallest velocity errors (b) occur for HARM averaging from marker to center points (grouping due to first interpolation step) or without markers HARM averaged center2node interpolation.

The dependence on viscosity interpolation methods for pressure and velocity solution is clearly visible (Figs. 11 and 13). Errors differ up to one order of magnitude for various viscosity interpolation methods. However, differences between the three FD formulations are very small. Staggered grid and stream function FDM follow the same trend with only a minor shift, independent of the interpolation procedure. The pressure solution for the rotated staggered grid FDM is in the range of the best results of the other two FDM. This result is not entirely surprising due to the advantage that viscosity does not need to be interpolated (see Section 4.1.3). The velocity solution is in the intermediate range. If markers are implemented for interpolation from markers to center points, results improve slightly for geometric and harmonic averaging methods (where harmonic averaging is slightly better), but not for an arithmetic averaging.

Applying none of the interpolation methods for the staggered grid FDM but defining viscosity directly at both center and nodal points results in slightly more accurate pressures than for the ARITH averaged viscosity (no markers) (Fig. 13, gray solid line). Nevertheless, the pressure errors are larger than for most of the averaging methods. The velocity error is in the intermediate range.

Results obtained with the FEM largely depend on whether the grid follows jumps in material properties or not (Fig. 14). If the grid exactly fits the inclusion, results are superior to those obtained with FDM and converge quadratically with increasing resolution. If the grid does not exactly follow the inclusion, averaging of viscosity from markers to integration points becomes important and harmonic averaging yields the most accurate results. The overall accuracy in those cases is comparable to the accuracy of FDM. The pseudo-adapted method (methods explained in Fig. 14(a)) which makes an attempt to increase the number of elements around phase boundaries, yields more accurate results than non-fitted, pseudo-regular mesh methods. If viscosity is sampled directly at integration points, errors in velocity and pressure are an order of magnitude larger than those obtained with the least accurate FDM. A possible explanation for this observation is that the $Q_2 - P_1$ elements used here assumes pressure to vary in a linear manner at most. Jumps in material properties result in discontinuous pressures, and approximating discontinuities with linear functions might result in a serious overestimation of pressures. This way of sampling viscosity should thus be avoided.

7.1.5. *Effect of viscosity contrast*

The effect of the viscosity contrast on the accuracy of numerical solutions is systematically tested for cases that go from a rigid inclusion (viscosity contrast $\mu_{\text{clast}}/\mu_{\text{matrix}} = 10^5$) to a weak inclusion (viscosity contrast $\mu_{\text{clast}}/\mu_{\text{matrix}} = 10^{-5}$). Numerical resolution is 200×200 grid points and 20×20 markers.

Here, we employ another type of error to get information about the maximum pressure compared to the analytical solution, a so called overshoot. The overshoot is the difference between the maximum pressure of the numerical and the maximum pressure of the analytical solution normalized by the maximum pressure of the analytical solution:

$$\text{Overshoot} = \frac{\|P_{\text{num}}\|_{\text{inf}} - \|P_{\text{ana}}\|_{\text{inf}}}{\|P_{\text{ana}}\|_{\text{inf}}}. \tag{47}$$

Results (Fig. 15) are only shown for the reference interpolation methods. Pressure overshoots generally occur for rigid inclusions and are generated at the clast–matrix boundary (see Section 7.1.1). Some interpolation methods (e.g. ARITH averaged solution) have errors up to 160%. Weak inclusions generally show pressure under-

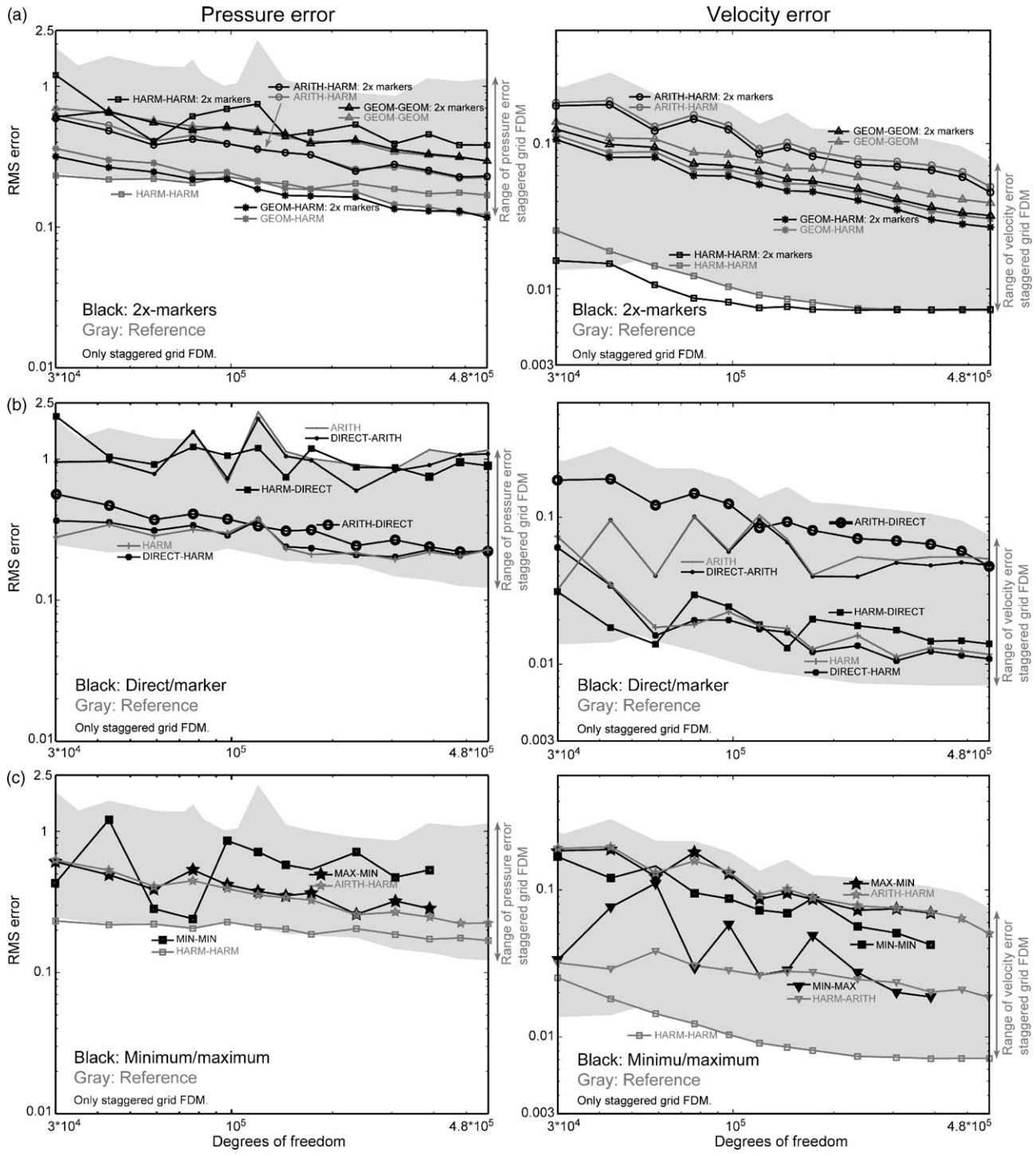

Fig. 12. RMS error of pressure and velocity as a function of resolution for (a) 2-time-marker, (b) direct/marker and (c) minimum/maximum viscosity interpolation methods (circular inclusion test). The descriptions of the viscosity interpolation methods and nomenclature is given in Fig. 7. The gray area shows the range of the results of the staggered grid FDM using the reference interpolation methods. None of these interpolation methods is significantly better. (a) The 2-times-marker method twice harmonically averaged (HARM–HARM 2×-markers) is only for the velocity solution slightly better but not for the pressure, which is interesting since it is expected that this method might represent the findings of the 1D analysis. (b) The good correlation between DIRECT-HARM direct/marker and HARM reference solutions show that principally markers do not affect the results. (c) Minimum/maximum solutions generally show no clear improvements related to the reference-methods. Further details are described in the text.

shoots (negative overshoot values) except for the rotated staggered grid and the HARM–HARM averaged staggered grid FD simulations.

It is most likely that these large overshoots occur due to pressure oscillations at the clast–matrix boundary. These oscillations might be numerical artifacts: depending on the interpolation method, it might happen that, in certain cells at the clast–matrix boundary, calculations are made by using much too high viscosity values instead of low (or vice versa). That is, numerically, the cell is inside of the clast but analytically it should be outside of the clast (or vice versa). The results show that such numerically induced errors

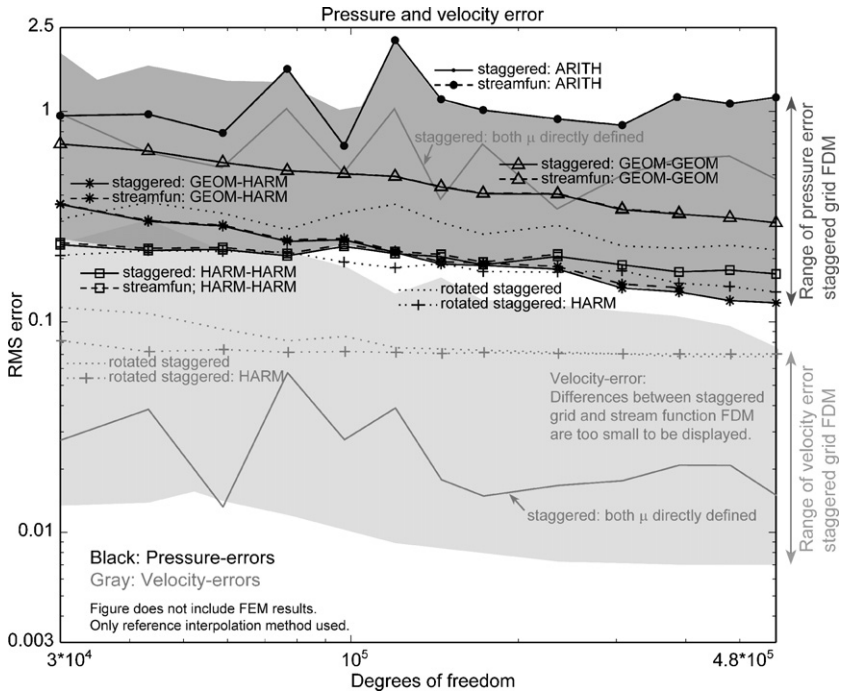

Fig. 13. RMS error as a function of resolution for different FD formulations and reference interpolation methods for viscosity (circular inclusion test). Pressure error (top) with worst result (ARITH), two best results (GEOM–HARM, HARM–HARM), and intermediate result (GEOM–GEOM). Velocity errors are almost one order of magnitude less than pressure errors (for the corresponding viscosity interpolation methods). Accuracies between different viscosity interpolation methods change up to almost one order of magnitude. Errors between staggered grid and stream function FDM are very small, for the velocity error the difference is not visible. Pressure errors of the rotated staggered grid FDM are small, while the velocity error is intermediate.

achieve much higher values for strong than for weak inclusions. Therefore, care has to be taken, since strong pressure gradients can induce flow.

7.2. Rayleigh–Taylor instability test

Numerical simulations for the simple two-layer model with a heavy top layer overlying a lighter bottom layer were performed. The system is driven by an initial perturbation of one wavelength. The induced velocity field is compared with the analytical solution (Biot, 1961; Biot and Odé, 1965; Whitehead, 1988). The maximum amplitude of the interface of $A_0 = 0.001H$ is smaller than the grid resolution. To drive the system the perturbation must be numerically visible. This problem was solved by implementing 20×20 markers to derive the volume fractions in the cells where the interface passes through. Therefore markers also carry the density information. This means that, in addition to viscosities, also densities are interpolated from markers to the corresponding density position in the FD grids (Fig. 6). This is different than for the circular inclusion test where only viscosities were averaged (density was constant). Viscosities, for this test, were interpolated with the reference interpolation methods (Fig. 7). Other methods exist (e.g. Level-set, boundary integral, volume-of-fluid methods) which can be used to track free surfaces, but for the sake of consistency between the circular inclusion and the Rayleigh–Taylor test the marker method was used.

7.2.1. Comparison of the tree finite difference methods

Unlike the circular inclusion test, the results of the Rayleigh–Taylor instability test are generally independent of the viscosity interpolation method (Fig. 16). The interpolation of density is extremely important to approximate the interface ideally. Results with an ARITH averaged density and any type of viscosity interpolation leads to the best results. All three FDM, staggered grid, stream function and rotated staggered grid FDM have very similar accuracies.

7.2.2. Effect of viscosity contrast

The effect of viscosity contrast on the accuracy of numerical simulations is shown in Fig. 17. Numerical resolution was 129×129 grid points and 20×20 markers per cell.

Results generally show overshoots except for the rotated staggered grid FDM. The trend for all methods is the same, a decrease of error close to a viscosity contrast of 1 ($\mu_{top} = \mu_{bottom}$). The stream function FDM show slightly better results than the staggered grid FDM. The staggered grid and stream function FDM show best results for ARITH averaged density irrespective of the viscosity interpolation. For high or low ($\geq 10^3$ or $\leq 10^{-3}$) viscosity contrasts a harmonic average for the second viscosity interpolation (HARM averaged viscosities from center to nodal points) have significantly larger errors. For this specific resolution (129×129) the rotated staggered grid FDM with GEOM averaged viscosity (markers to center points) has very small errors but they increase for higher resolutions (Fig. 16). The rotated staggered grid with an ARITH averaged viscosity has almost the same accuracy as the stream function FDM with an ARITH averaged density.

8. Discussion

The analysis presented here demonstrates how material properties are defined in different FD formulations in presence of strongly varying material properties, in particular viscosity. Quantitatively it was shown that the accuracy of the pressure (circular inclusion test) or velocity solution (circular inclusion and Rayleigh–Taylor instability test) is critically dependent on the averaging scheme. We also demonstrated, that certain arrangements of elements in FEM show

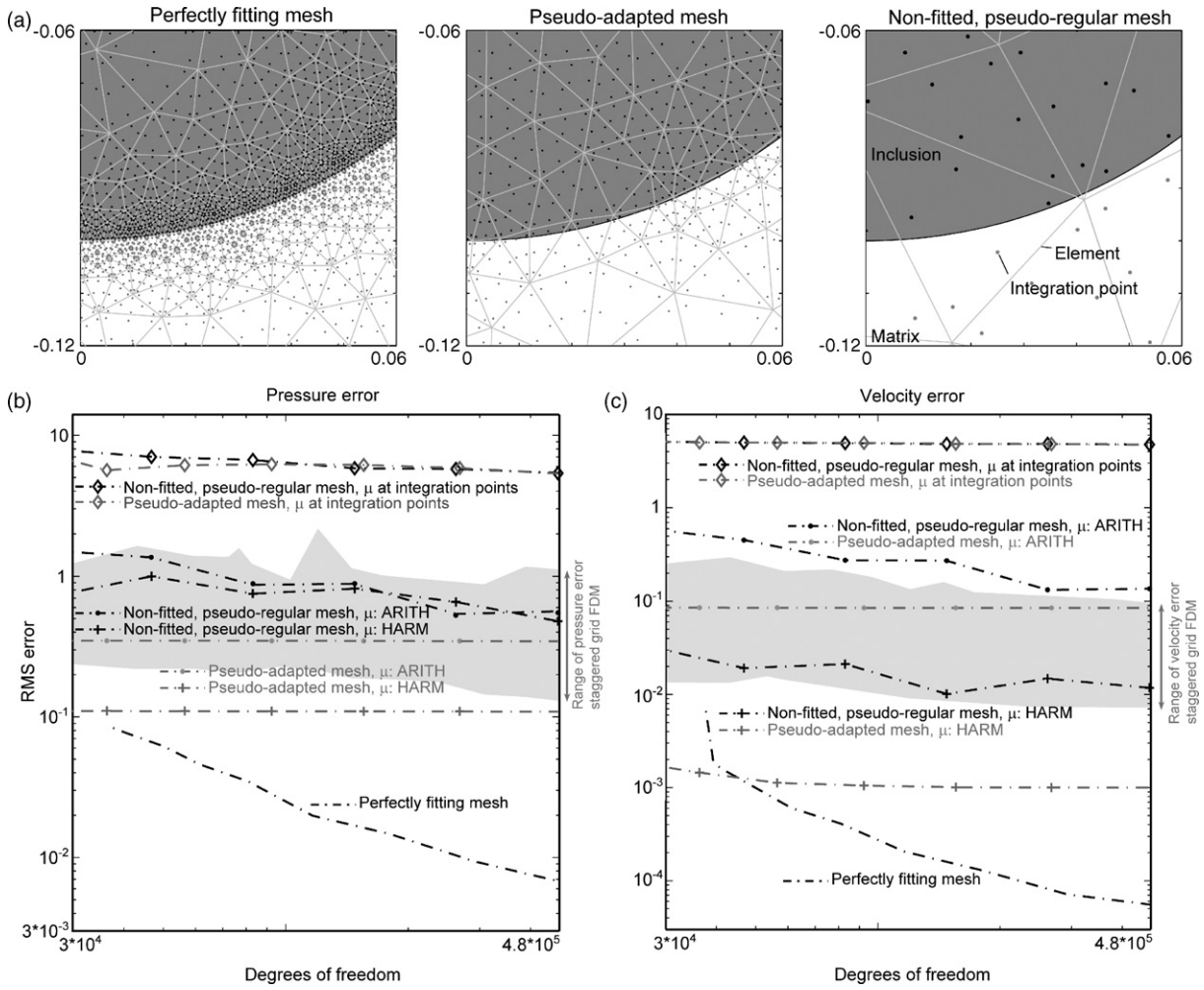

Fig. 14. RMS error as a function of resolution for FEM (circular inclusion test). (a) Different mesh generation techniques that have been employed in the test (each one has ≈ 30000 degrees of freedom). Element boundaries, location of integration points and location of the inclusion are indicated. The perfectly fitting mesh creates elements that exactly follow the inclusion boundary. The pseudo-adapted mesh, interpolates material properties from marker-distributions to a regular grid and computes jumps in material properties from this grid. The non-fitted, pseudo-regular mesh creates elements that have approximately the same area throughout the computational domain. Integration points within an element may have different viscosities in the pseudo-adapted and non-fitted, pseudo-regular mesh case. If this occurs, the viscosity in an element might be averaged elementwise (using harmonic or arithmetic averaging) or might be sampled directly at the integration points. (b) Pressure error vs. resolution for various grids and element-averaging methods. The perfectly fitting mesh method clearly yields the best results; the other methodologies have an accuracy that is comparable to that of FD techniques (gray area) if viscosity is averaged over the element. If viscosity is sampled directly at integration points, the results are less accurate than that of FD techniques. (c) Velocity error vs. resolution.

large differences in accuracies and have the same error amplitudes as FDM.

8.1. 1D analytical and numerical effective viscosity study

Problems generally arise due to the fact that material interfaces can only be resolved in a discrete manner. In the present analysis the interface of the circular inclusion is always bisecting cells. The question addressed in this work is how material properties (here viscosity) should be defined if significant changes occur within a cell.

A 1D analytical solution was derived for a simple setup to compute an effective (optimal) viscosity in a cell where two different materials are present. Marker ratio harmonic averages for the viscosity represented the analytical solution very well. Simple viscosity averaging (without markers) are dependent on the location of the interface and the sign of the viscosity gradient which is in difference to the marker ratio method.

Applying the findings of the 1D analysis directly in 2D is not straightforward. For the 2D FD formulations, it was expected that a double harmonic marker averaging, once from marker to center and once from marker to nodal points, yields the best results. Interestingly, this was only the case for the velocity solution and improvements were only minimal. This disagreement might be explained by the order of the derivatives: velocities are solved by second order derivatives, while pressure is only a first order derivative, additionally, in 1D we only solve for velocity solutions. Results using direct/marker or minimum/maximum viscosities interpolation methods do not show better results as the ones produced by the reference interpolation methods (for definitions of methods see Fig. 7).

8.2. 2D numerical models

One major reason that the generalization from the 1D to the 2D solutions is not straightforward might be due the different viscosity positions one has to deal with in 2D FD formulations (staggered grid and the stream function FDM). One location is in the center and one at nodal points of a cell. The 2D numerical results for the setup of the circular inclusion, however, indicate that a combination of marker-based harmonic viscosity averaging to center points with

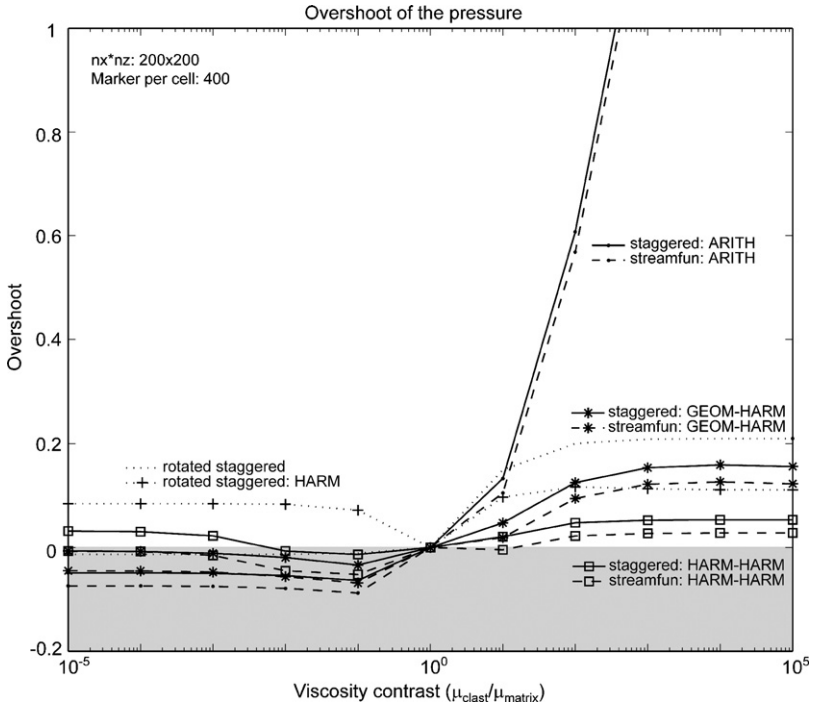

Fig. 15. Overshoot (Eq. (47)) vs. viscosity contrast $\mu_{\text{clast}}/\mu_{\text{matrix}}$ for the three different FD techniques for the circular inclusion test. Gray region represents region of undershoot (i.e. the maximum pressure of the numerical solution is smaller than the maximum pressure of the analytical solution).

harmonic averaging from center to nodal points is advisable. The Rayleigh–Taylor instability test yields different results: here, arithmetic interpolation of densities gives the best results. These differences are most likely due to different model setups, in particular how the systems are driven (kinematic or buoyancy/stress driven). Moreover, in the Rayleigh–Taylor instability test, resolving the interface is of major importance, and averaging density has a more important effect on the overall accuracy than averaging of viscosity. This might be due to the fact that such an interface is preferable represented by real volumetric fractions, which is an arithmetic mean of two different material properties. Another explanation is that the velocities of the Rayleigh–Taylor instabilities are related to the density contrast and are influenced only globally by the viscosity contrast, while in the circular inclusion test the pressure distribution is directly dependent on the local viscosity contrast and the velocity distribution in turn is dependent on the pressure.

Differences between the three FD schemes are secondary compared to the manner in which viscosity or density are interpolated. For both model setups (circular inclusion or two-layer model) different averaging procedures cause significantly different results

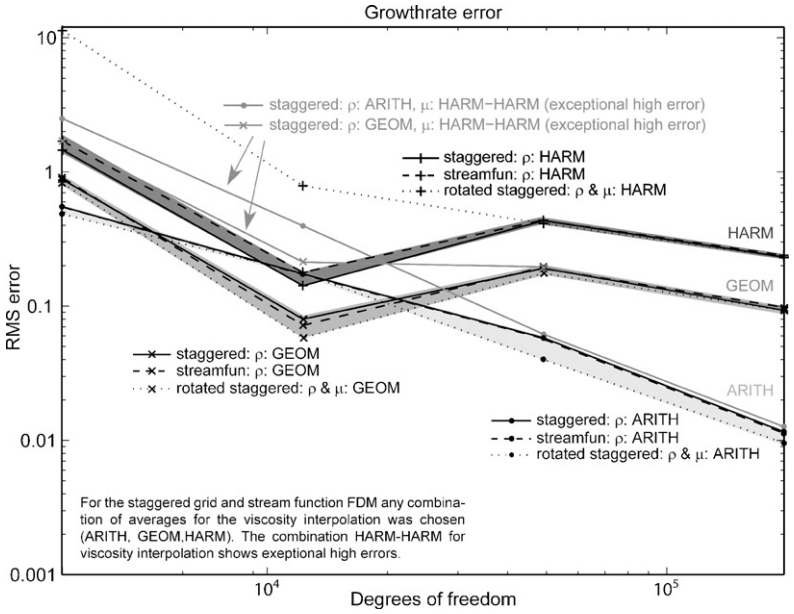

Fig. 16. RMS error of growthrate (Eq. (46)) as a function of resolution for different density and viscosity interpolation methods for the Rayleigh–Taylor instability test. The density interpolation is the factor, which groups the results. For the viscosity the reference interpolation methods were used. The combination of the viscosity averages has almost no effect on the results, except the HARM–HARM averages show very high errors. ARITH averaged density yields best results.

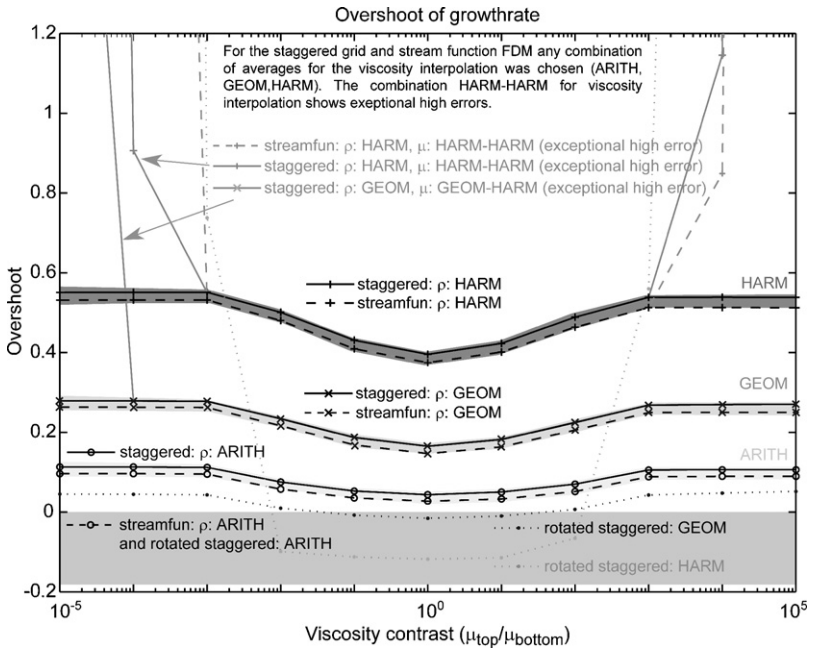

Fig. 17. Overshoot (Eq. (47)) vs. viscosity contrast μ_{top}/μ_{bottom} for the three different FD techniques for the Rayleigh–Taylor instability test. The density interpolation is the factor, which groups the results. For the viscosity the reference interpolation methods were used. The combination of the viscosity averages has almost no effect on the results, except the HARM–HARM or GEOM–HARM averages show very high errors. Grey bar represents region of undershoot. ARITH averaged density yields best results.

and accuracy can change up to one order of magnitude. The similarity between results of the staggered grid and the stream function FDM might be due to the way that pressure is determined for the stream function formulation. Integration of the force balance equations (Eqs. (37) or (38)) for pressure results in the same staggered positions for velocities and pressure as for the staggered grid FDM. The good results of the rotated staggered grid FDM might be due to the fact that no center to nodal point viscosity interpolation is necessary. In this case the findings of the 1D analysis seem to extend well to the 2D case.

The problem of averaging of material properties was also considered by Moczo et al. (2002) for the case of a 3D heterogeneous staggered grid FD model of seismic wave propagation with discontinuous material parameters such as the elastic moduli and densities. They obtained, in the 1D case, a similar result and found that the elastic coefficient should be harmonically averaged whereas densities should be arithmetically averaged. An other interesting study (Moskow et al., 1997) considering nonconforming Cartesian grid to interfaces using elliptic equations discusses two averaging schemes, which are dependent on the direction of anisotropy and can only be applied to very simplified setups. They use arithmetic averages in directions parallel to a layering (creating the anisotropy) and harmonic averages perpendicular to the layering (direction of changes). The methodology might potentially also be useful for solving variable viscosity Stokes problems.

8.3. *Different numerical methods*

The problem of numerically induced artifacts such as oscillations or checkerboard pressures along high viscosity contrasts could, theoretically, be largely resolved by using Lagrangian FEM in which the elements exactly follow the boundaries of viscosity contrast. We demonstrated the success of such an approach for the very simple setup of a strong circular inclusion. But already small deviations from a perfectly fitting mesh such as the pseudo-adapted or the non-fitted, pseudo-regular meshing methods, where jumps in viscosity occur within an element, yield accuracies which are at best equal to those of FDM. These findings are in agreement with those of Moresi et al. (1996), who demonstrated that viscosity contrasts that occur inside an element may result in large errors in pressure, whereas viscosity contrasts that occur along element boundaries yield sufficiently accurate results.

Additionally, the results also show that direct sampling of viscosity at integration points might seriously degrade the accuracy of the overall solution if sharp jumps are present, and should thus be avoided. It is possible that this result is an artifact of the use of higher-order elements, since the linear approximation for pressure might result in overshoots at discontinuities. Future tests with linear elements, such as the $Q_1 - P_0$ element, are required to better understand this phenomenon. Initial test results, obtained with GALE, indicate that similar issues occur in this case (Landry et al., 2008). The results here also show that marker-in-cell FEM, in which material properties are defined at markers and integration points move with markers, could suffer from similar problems if sharp jumps in properties occur.

A number of techniques have the potential to overcome some of the problems described here. A split-element technique could be applied that effectively splits the element in two if sharp gradients occur (e.g. Braun et al., this issue). Gradient recovery techniques might improve the pressure accuracy in a post-processing step (Sharples et al., 2006). Extended FE techniques can be used, that adds degrees of freedom at the location of the discontinuity (Belytschko et al., 2001; Jäger et al., 2008). So far, however, none of these techniques seem to have been compared with analytical solutions such as the ones presented here. Moreover, some techniques might be difficult to extend to three dimensions. More work is thus required to evaluate the full potential of those methods.

Beside the fact that Lagrangian FEM techniques show very good accuracies, there are reasons why Eulerian techniques are likely to remain popular in computational geodynamics. Typical lithospheric-scale problems require modeling of extreme deformations alongside large variations in material properties. Such problems could, in theory, be solved with an unstructured FEM,

which automatically adapts the grid to every jump in material properties. In practice, this is nearly impossible since interfaces and layers may have a fairly fine structure or may evolve into extremely fine-structured features. Resolving this numerically and ensuring that triangular elements have a close-to-optimal shape requires a lot of elements, in particular, since layers might undergo significant stretching and folding during the course of simulation (Gorczyk et al., 2007). Typically, extremely fine-scaled patterns emerge from relative simple initial structures. This means that the number of elements increases significantly during the simulation, which might therefore require a lot of memory and cpu-time.

8.4. Pressure accuracy

A purpose of the present analysis is to address the question of whether the pressure solution has sufficient accuracy for solving coupled systems such as two-phase flow models, where the pressure feeds back to the solution. The analysis of the overshoot versus viscosity contrast for circular inclusions shows that the accuracy of the pressure is particularly problematic for highly viscous inclusions. Pressure solutions have oscillations around the clast–matrix boundary. Models of two-phase flow (e.g. melt migration through the mantle) are more likely to resemble the opposite case in which a lower viscosity fluid is embedded in a solid, viscously deformable matrix. For this case the maximum pressures of the numerical solution are mostly slightly smaller than that of the analytical solution. This might thus be less of a numerical issue. Generally, the pressure gradient at locations of pressure oscillations can achieve much higher values for strong than for weak inclusions. This gradient can induce fast flow, which is the consequence of numerical artifacts. This overshoot can drastically be reduced by using an appropriate viscosity interpolation method. Nevertheless, differences between different setups should be considered when choosing one of the presented interpolation schemes.

9. Conclusions

In this paper we have analyzed the effects of viscosity averaging and numerical methodology on the accuracy of the Stokes equations in the presence of viscosity variations.

In 1D analytical and numerical tests, we demonstrated that the optimal viscosity in a cell, where an interface is separating two domains of different viscosities, is a harmonic average weighted according to the fractions of the two viscosities. The harmonically marker ratio average could represent the solution very well, while, on the other hand, a simple harmonic average from nodal to center points is dependent on the location and the sign of the viscosity contrast.

In 2D numerical tests using FDM, we showed that for a setup of a circular inclusion in a domain with kinematic boundary conditions, a marker-based harmonic averaging to center points and a harmonic averaging from center to nodal points yields best results. For the pressure solutions, however, a geometric averaging to center points and a harmonic averaging from center to nodal points is slightly better for higher resolutions. Errors in velocity are always about an order of magnitude smaller than errors in pressure. However, for a buoyancy/stress driven system such as the Rayleigh–Taylor instability test, the results are dominated by the density interpolation and not by the viscosity interpolation. In this case an arithmetic averaging for density must be applied while the viscosity interpolation can have any type of averaging scheme. The differences between various numerical methodologies for both setups are small compared to the differences between various viscosity or density averaging schemes.

Viscosity interpolation methods are thus of crucial importance in modeling geodynamic problems with FDM, particularly if the dynamic pressure is of interest. While an ideal Eulerian numerical method does not seem to exist, one can improve the accuracy of such approaches by choosing the correct averaging method. We also demonstrate that a Lagrangian FEM for geodynamic problems with highly varying viscosity would be an appropriate tool but only if the elements perfectly fit the material boundaries. Problems can arise if large deformations should be modeled. Eulerian FE models have the same accuracies as the FD models or in case of direct material sampling at integration points results are one order of magnitude worse. Therefore, Eulerian approaches such as the FDM remain useful. On the basis of the tests performed here using FDM, we recommend the use of a harmonic averaging from marker to center points and a harmonic averaging from center to nodal points. In presence of density variations, densities are preferably marker-based arithmetically averaged. This findings were successfully applied for a free subduction benchmark study (Schmeling et. al, this issue).

Acknowledgements

This work was supported by the Swiss National Science Foundation grant 200021-107889. Helpful comments on the manuscript of James Connolly and Stefan Schmalholz are gratefully acknowledged. We thank Taras Gerya and Erik Saenger for stimulating discussions. We further thank the reviewers R. Katz and M. Krotkiewski and the editor D. Schmid for insightful and helpful reviews.

References

Albers, M., 2000. A local mesh refinement multigrid method for 3D convection problems with strongly variable viscosity. Journal of Compuational Physics 160 (1), 126–150.
Auth, C., Harder, H., 1999. Multigrid solution of convection problems with strongly variable viscosity. Geophysical Journal International 137, 793–804.
Belytschko, T., Moes, N., Usui, S., Parimi, C., 2001. Arbitrary discontinuitites in finite elements. International Journal for Numerical Methods in Engineering 50 (4), 993–1013.
Biot, M., 1961. Theory of folding of stratified viscoelastic media and its implications in tectonics and orogenesis. Geological Society of America Bulletin 72, 1595–1620.
Biot, M., Odé, H., 1965. Theory of gravity instability with variable overburden and compaction. Geophysics 30, 153–166.
Braun, J., Sambridge, M., 1994. Dynamic Lagrangian remeshing (DLR): a new algorithm for solving large strain deformation problems and its application to fault-propagation folding. Earth and Planetary Science Letters 124, 211–220.
Buiter, S.J.H., Babeyko, A., Ellis, S., Gerya, T., Kaus, B., Kellner, A., Schreurs, G., Yamada, Y., 2006. The numerical sandbox: comparison of model results for a shortening and an extension experiment. In: Buiter, S.J.H., Schreurs, G., (Eds.), Analogue and Numerical Modelling of Crustal-Scale Processes, vol. 253. Geological Society of London Special Publications, Geological Society of London, pp. 29–64.
Burg, J.P., Gerya, T.V., 2006. The role of viscous heating in barrovian metamorphism of collisional orogens: thermomechanical models and application to the lepontine dome in the central alps. Journal of Metamorphic Geology 23, 75–95.
Burg, J.P., Kaus, B., Podladchikov, Y., 2004. Dome structures in collision orogens mechanical investigation of the gravity/compression interplay. In: Whitney, D., Teyssier, C., Siddoway, C. (Eds.), In: Gneiss Domes in Orogeny, vol. 380. Geological Society of America, Boulder, pp. 47–66.
Choblet, G., 2005. Modelling thermal convection with large viscosity gradients in one block of the "cubed sphere". Journal of Computational Physics 205 (1), 269–291.
Connolly, J.A.D., Podladchikov, Y., 2007. Decompaction weakening and channeling instability in ductile porous media: implications for asthenospheric melt segregation. Journal of Geophysical Research.
Cuvelier, C., Segal, A., van Steemhoven, A., 1986. Finite element methods and Navier–Stokes equations. In: Mathematics and its Applications. Reidel Publishing Company, Dordrecht.
Dabrowski, M., Krotkiewski, M., Schmid, D.W., 2008. MILAMIN: MATLAB-based FEM solver for large problems. Geochem. Geophys. Geosyst., doi:10.1029/2007GC001719.
Elman, H., Silvester, D., Wathen, A., 2005. Finite elements and fast iterative solvers with applications to incompressible fluid dynamics. In: Numerical Mathematics and Scientific Computation. Oxford University Press.
Fletcher, C., 1991. Computational Techniqus for Fluid Dynamics, vol. 2. Springer.
Fullsack, P., 1995. An arbitrary Lagrangian–Eulerian formulation for creeping flows and its application in tectonic models. Geophysical Journal International 120 (1), 1–23.

Gerya, T.V., Yuen, D., 2003. Characteristics-based marker-in-cell method with conservative finite-differences schemes for modeling geological flows with strongly variable transport properties. Physics of the Earth and Planetary Interiors 140, 293–318.
Gerya, T.V., Yuen, D., 2007. Robust characteristics method for modelling multiphase visco-elasto-plastic thermo-mechanical problems. Physics of the Earth and Planetary Interiors.
Gorczyk, W., Gerya, T., Connolly, J., Yuen, D., 2007. Growth and mixing dynamics of mantle wedge plumes. Geology 35, 587–590.
Huismans, R.S., Beaumont, C., 2002. Asymmetric lithospheric extension: the role of frictional plastic strain softening inferred from numerical experiments. Geology 30 (3), 211–214.
Jäger, P., Steinmann, P., Kuhl, E., 2008. On local tracking algorithms for the simulation of three-dimensional. Comput. Mech. 42, 395–406.
Jamieson, R., Beaumont, C., Nguyen, C.H., Grujic, D., 2006. Provenance of the greater himalayan sequence and associated rocks: predictions of channel flow models. In: Law, R., Searle, M., Godin, L. (Eds.), In: Channel Flow, Ductile Extrusion and Exhumation of Lower-Mid Crust in Continental Collision Zones, vol. 268. Geological Soc. London Spec. Publ.
Kameyama, M., Kageyama, A., Sato, T., 2005. Multigrid iterative algorithm using pseudo-compressibility for three-dimensional mantle convection with strongly variable viscosity. Journal of Computational Physics 206, 162–181.
Katz, R.F., Knepley, M.G., Smith, B., Spiegelman, M., Coon, E., 2007. Numerical simulation of geodynamic processes with the portable extensible toolkit for scientific Computation. Physics of th Earth and Planetary Interiors 163 (1–4), 52–68.
Katz, R.F., Spiegelman, M., Holtzman, B., 2006. The dynamics of melt and shear localization in partially molten aggregates. Nature 442, 676–679.
Kaus, B., Podladchikov, Y., Schmid, D.W., 2004. Eulerian spectral/finite difference method for large deformation modelling of visco-elasto-plastic geomaterials. Bolletino Geofisico 45, 346–349.
Kaus, B.J.P., Podladchikov, Y., 2006. Initiation of localized shear zones in viscoelastoplastic rocks. Journal of Geophysical Research 111 (B04412).
Landry, W., Hodkinson, L., Kientz, S., 2008. GALE User Manual, Version 1.2.2. http://www.geodynamics.org/cig/software/packages/long/gale.
Mancktelow, N.S., 2006. How ductile are ductile shear zones? Geology 34 (5), 345–348.
McKenzie, D.P., 1984. The generation and compaction of partially molten rock. Journal of Petrology 25 (3), 713–765.
Moczo, B., Kristek, J., Vavrycuk, V., Archuleta, R., Halada, L., 2002. 3D heterogeneous staggered-grid finite difference modelling of seismic motion with volume harminic and arithmetic averaging of elastic moduli and densities. Bulletin of the Seismological Society of America 93, 3042–3066.
Morency, C., Huismans, R., Beaumont, C., Fullsack, P., 2007. A numerical model for coupled fluid flow and matrix deformation with applications to disequilibrium compaction and delta stability. Journal of Geophysical Research 112.
Moresi, L., Dufour, F., Mühlaus, H.B., 2002. Mantle convection modeling with viscoelastic/brittle lithosphere: numerical modeling and plate tectonic modeling. Pure and Applied Geophysics 159, 2335–2356.
Moresi, L., Dufour, F., Mühlhaus, H.B., 2003. A Lagrangian integration point finite element method for large deformation modeling of viscoelastic geomaterials. Journal of Computational Physics 184, 476–497.
Moresi, L., Quenette, V., Lemiale, V., Meriaux, C., Appelbe, B., Mühlhaus, H.B., 2007. Computational approaches to studying non-linear dynamics of the crust and mantle. Physics of the Earth and Planetary Interiors 163.
Moresi, L., Solomatov, V., 1995. Numerical investigations of 2D convection in a fluid with extremely large viscosity variations. Physics of Fluids 7, 2154–2162.
Moresi, L., Zhong, S., Gurnis, M., 1996. The accuracy of finite element solutions of Stokes's flow with strongly varying viscosity. Physics of the Earth and Planetary Interiors 97 (1–4), 83–94.
Moskow, S., Druskin, V., Habashy, T., Lee, P., Davydycheva, S., 1997. A finite difference scheme for elliptic equations with rough coefficients using a Cartesian grid nonconforming to interfaces. SIAM Journal on Numerical Analysis 36 (2), 442–464.
Mühlhaus, H., Bourgouin, L., Hale, A., 2007. Free surfaces modeling based on Level sets. International Conference on Computational and Experimental Engineering and Sciences 3 (4), 225–232.
Petrini, K., Podladchikov, Y., 2000. Lithospheric pressure–depth relationship in compressive regions of thickened crust. Journal of Metamorphic Geology 18 (1), 67–77.
Ranalli, G., 1995. Rheology of the Earth, 2nd ed. Chapman and Hall, London.
Saenger, E., Bohlen, T., 2004. Anisotropic and viscoelastic finite-difference modeling using the rotated staggered grid. Geophysics 69 (2), 583–591.
Saenger, E., Gold, N., Shapiro, S., 2000. Modeling the propagation of elastic waves using a modified finite-difference grid. Wave Motion 31, 77–92.
Schmalholz, S.M., Podladchikov, Y.Y., Schmid, D.W., 2001. A spectral/finite difference method for simulating large deformations of heterogeneous, viscoelastic materials. Geophysical Journal International 145 (1), 199–208.
Schmeling, H., Jacoby, W.R., 1981. On modelling the lithosphere in mantle convection with nonlinear rheology. Journal of Geophysics 50, 89–100.
Schmid, D.W., 2002. Finite and Infinite Heterogeneities Under Pure and Simple Shear. PhD. Swiss Federal Institute of Technology.
Schmid, D.W., Podladchikov, Y., 2003. Analytical solutions for deformable elliptical inclusions in general shear. Geophysical Journal International 155, 269–288.
Schott, B., Yuen, D.A., Schmeling, H., 2000. The diversity of tectonics from fluid-dynamical modeling of the lithosphere–mantle system. Tectonophysics 322 (1–2), 35–51.
Schubert, G., Olson, P., Turcotte, D.L., 2001. Mantle Convection in the Earth and Planets. Cambridge University Press.
Scott, D., 1988. The competition between percolation and circulation in a deformable porous medium. Journal of Geophysical Research 93 (B6), 6451–6462.
Scott, D., Stevenson, D.J., 1986. Magma ascent by porous flow. Journal of Geophysical Research 91, 9283–9296.
Sharples, W.K., Moresi, L.N., May, D.A., Giordani, J., Lemiale, V., 2006. Gradient recovery methods for improved stresses and strain rates in geodynamic models. Eos Trans. AGU, Fall Meet. Suppl. 87 (52), abstract T13C–530.
Shaw, H., 1969. Viscosity of basalt in the melting range. Journal of Petrology 10, 510–535.
Spiegelman, M., 2003. Linear analysis of melt band formation by simple shear. Geochemistry Geophysics Geosystems 4 (9), 8615.
Sussman, M., Smereka, P., Osher, S., 1994. A level set approach for computing solutions to incompressible two-phase flow. Journal of Computational Physics 114 (1), 146–159.
Tackley, P., 2000. Self-consistent generation of tectonic plates in time-dependent, three-dimensional mantle convection simulations. 1. Pseudoplastic yielding. Geochem. Geophys. Geosyst. 01 (23).
Tackley, P., King, S.D., 2003. Testing the tracer ratio method for modeling active compositional fields in mantle convection simulations. Geochem. Geophys. Geosyst. 4 (4).
Tannehill, J.C., Anderson, D.A., Pletcher, R.H., 1997. Computational fluid mechanics and heat transfer. Series in Computational and Physical Processes in Mechanics and Thermal Sciences.
Toussaint, G., Burov, E., Avouac, J.P., 2004. Tectonic evolution of a continental collision zone: a thermomechanical numerical model. Tectonics 23, TC6003.
Trompert, R., Hansen, U., 1996. The application of a finite volume multigrid method to 3D flow problems in a highly viscous fluid with variable viscosity. Geophysical and Astrophysical Fluid Dynamics 83, 261.
Turcotte, D.L., Schubert, G., 1982. Geodynamics. Wiley.
Vasilyev, O.V., Podladchikov, Y.Y., Yuen, D.A., 2001. Modeling of plume-lithosphere interaction using adaptive multilevel wavelet collocation algorithm. Geophysial Journal International 147 (3), 579–589.
Vermeer, P.A., 1990. The orientation of shear bands in bi-axial tests. Geotechnique 40 (2), 223–236.
Weinberg, R.F., Schmeling, H., 1992. Polydiapirs: multiwavelength gravity structures. Journal of Structural Geology 14 (4), 425–436.
Whitehead, J., 1988. Fluid models of geological hotspots. Annual Reviews 20, 61–87.
Zhong, S., Yuen, D., Moresi, L., 2007. Numerical methods in mantle convection. Treatise in Geophysics 7, 227–252.